© 2015. Published by The Company of Biologists Ltd | Development (2015) 142, 4329-4339 doi:10.1242/dev.124750

RESEARCH ARTICLE

# Asymmetric cell convergence-driven zebrafish fin bud initiation and pre-pattern requires Tbx5a control of a mesenchymal Fgf signal

**Qiyan Mao[1,*], Haley K. Stinnett[2] and Robert K. Ho[2,‡]**

## ABSTRACT

Tbx5 plays a pivotal role in vertebrate forelimb initiation, and loss-of-function experiments result in deformed or absent forelimbs in all taxa studied to date. Combining single-cell fate mapping and three-dimensional cell tracking in the zebrafish, we describe a Tbx5a-dependent cell convergence pattern that is both asymmetric and topological within the fin-field lateral plate mesoderm during early fin bud initiation. We further demonstrate that a mesodermal Fgf24 convergence cue controlled by Tbx5a underlies this asymmetric convergent motility. Partial reduction in Tbx5a or Fgf24 levels disrupts the normal fin-field cell motility gradient and results in anteriorly biased perturbations of fin-field cell convergence and truncations in the pectoral fin skeleton, resembling aspects of the forelimb skeletal defects that define individuals with Holt–Oram syndrome. This study provides a quantitative reference model for fin-field cell motility during vertebrate fin bud initiation and suggests that a pre-pattern of anteroposterior fate specification is already present in the fin-field before or during migration because perturbations to these early cell movements result in the alteration of specific fates.

**KEY WORDS: Limb-field (fin-field), Limb bud (fin bud), Lateral plate mesoderm, Cell migration, Chemoattractant, Tbx5a, Fgf24, Holt–Oram syndrome, Zebrafish**

## INTRODUCTION

The T-box transcription factor Tbx5 plays a pivotal role in vertebrate forelimb initiation (Agarwal et al., 2003; Ahn et al., 2002; Garrity et al., 2002; Ng et al., 2002; Rallis et al., 2003; Takeuchi et al., 2003). For example, human *TBX5* haploinsufficiency is associated with Holt–Oram syndrome (Basson et al., 1997; Li et al., 1997), in which affected individuals exhibit forelimb defects ranging from a reduction in the radius and the anterior-most digit (pre-axial hemimelia) to a complete loss of arm (phocomelia) (Basson et al., 1994; Holt and Oram, 1960; McDermott et al., 2005). The anteriorly biased reduction of the forelimb skeleton in Holt–Oram syndrome suggests a developmental patterning defect; however, the cellular behaviors affected by Tbx5 during limb bud initiation are unknown. Here, we have used zebrafish to investigate Tbx5a-dependent cell movements and the downstream genetic cascade that results in outgrowth and patterning of the early vertebrate limb bud.

[1]Committee on Development, Regeneration and Stem Cell Biology, University of Chicago, Chicago, IL 60637, USA. [2]Department of Organismal Biology and Anatomy, University of Chicago, Chicago, IL 60637, USA.
*Present address: Aix Marseille Université, CNRS, IBDM UMR7288 13009 Marseille, France.

‡Author for correspondence (rkh@uchicago.edu)

**Received 25 March 2015; Accepted 27 October 2015**

Knowledge of the cellular processes underlying limb bud initiation offers unique insights into the genetic mechanisms underlying normal or pathological limb development. Early histological studies suggested that on-site cell proliferation is the sole mechanism for supplying limb bud mesenchymal cells (Harrison, 1918; Rallis et al., 2003; Searls and Janners, 1971; Swett, 1923). However, subsequent investigations suggested a cell movement-based mechanism, in which limb-field cells segregate from flanking regions because of higher tissue cohesivity (Damon et al., 2008; Foty et al., 1996; Heintzelman et al., 1978). In zebrafish, lateral plate mesoderm (LPM) cells appear to migrate in a Tbx5a-dependent manner into the future pectoral fin bud region prior to overt fin bud formation (Ahn et al., 2002; Garrity et al., 2002). Moreover, oriented cell motility and divisions of limb bud cells have been reported during the early outgrowth of mouse and chick limbs and zebrafish fins (Wyngaarden et al., 2010). Recently, Tbx5-dependent epithelial-to-mesenchymal transition was observed within the presumptive limb-field in chick embryos (Gros and Tabin, 2014). Together, these data suggest a conserved function for Tbx5a in the promotion of oriented cell motility during limb bud initiation.

Tbx5 expression initiates a cascade of various Fibroblast growth factor (Fgf) signals in the limb mesenchyme (Agarwal et al., 2003; Ng et al., 2002; Takeuchi et al., 2003), which eventually induces Fgf8 in the apical ectodermal ridge, a structure essential for the maintenance of limb cell proliferation (Bénazet et al., 2009; Boulet et al., 2004; Lewandoski et al., 2000; Ohuchi et al., 1997). Although the importance of ectodermal Fgf signaling has been well documented (Boulet et al., 2004; Crossley et al., 1996; Lewandoski et al., 2000; Moon and Capecchi, 2000; Vogel et al., 1996), much less is known about the roles of the earlier mesodermal Fgf signals. In chicks, epithelial-to-mesenchymal transition of limb-field LPM cells requires mesodermal expression of the Tbx5 target Fgf10 (Gros and Tabin, 2014), and in zebrafish, formation of the fin bud from fin-field LPM cells requires mesodermal expression of the Tbx5a target Fgf24 (Fischer et al., 2003). Together, these findings suggest a role for early mesodermal Fgf signals in regulating LPM cell motility during limb bud formation. However, it remains unclear how or if mesenchymal Fgf signals promote oriented cell behaviors observed in the LPM during limb bud initiation.

In this study, we establish the mechanistic connection between Tbx5a, mesodermal Fgf signals and motility patterns in the zebrafish pectoral fin-field. We combine single-cell-resolution fate mapping and three-dimensional cell tracking to demonstrate definitively that zebrafish pectoral fin-field cells converge along the anteroposterior (AP) axis while maintaining their relative initial AP positions topologically to form the fin bud. Here, we use the term 'topological' to refer to an ordered process that maintains the initial organization of a group of precursor cells, or field of cells,

Development (2015) 142, 4329-4339 doi:10.1242/dev.124750

within the final tissue or organ. Our analyses show that LPM cells exhibit differences in cell motility that result in the asymmetric positioning of fin-field cells towards a defined location in the posterior fin-field. We further show that fin-field LPM cells can migrate towards an ectopic source of Fgf, supporting a role for Fgf24 in the posterior fin-field LPM as the convergence cue for fin bud precursors. Our study also uncovers an early AP pre-pattern within the pectoral fin-field. Partial knockdown of either Tbx5a or Fgf24 leads to a biased perturbation of the anterior fin-field cells, resulting in their failure to migrate into the fin bud. This preferential loss of anterior convergence results in anteriorly biased truncations of the pectoral fin disc in larval zebrafish that resemble aspects of the forelimb skeletal defects that define individuals with Holt–Oram syndrome and suggests that early fin-field cells contain positional identities prior to convergence.

## RESULTS

### A single-cell-resolution fate map reveals convergence of the pectoral fin-field in the zebrafish LPM

We define the zebrafish pectoral fin-field as the area within the LPM from which the mesenchymal cells of the pectoral fin bud are derived. To map the territory of the fin-field at single-cell resolution, single blastomeres in 64- to 128-cell-stage embryos were injected with *Kaede* mRNA (Ando et al., 2002). We then photo-converted from green to red fluorescence in individual LPM cells at 14 hours postfertilization (hpf) and followed the labeled progeny up to 48 hpf. Using flanking inter-somitic borders as landmarks, we constructed a fate map of the LPM region at 14 hpf consisting of 105 labeled single cells between somite levels 1 and 6 (Fig. 1E). We classified later progeny clones into four fate groups according to the location and morphology of the labeled progeny cells at 28-48 hpf. All clones of cells derived from single cells labeled at 14 hpf gave rise to progeny of only one fate type, as follows: (1) cardiac (Fig. 1A, $n$=6), consisting of one or two labeled cells located anterior to the common cardinal vein within either the myocardial or the pericardial tissue; (2) fin (Fig. 1B; $n$=72), labeled cells consisting of two to four progeny of irregular cuboidal morphology within the mesenchyme of the fin bud proper beneath the fin epidermis; (3) peritoneum (Fig. 1C; $n$=14), typically consisting of four progeny spreading laterally over the yolk sac; and (4) medial (Fig. 1D, $n$=13), consisting of one or two labeled cells located more medially than other labeled clones and within the position of the intermediate mesoderm. Thus, the mapped LPM region is roughly segregated into cardiac, fin and peritoneum fields from anterior to posterior (Fig. 1E). The fin-field at 14 hpf occupies a region within the LPM roughly 200 µm along the AP body axis (flanking somites 1-4; Fig. 1E, between red dashed lines), approximately 1.6 times the AP length of the pectoral fin bud at 28 hpf (~120 µm along the AP axis, flanking somites 2-3; Fig. 1E). This result is consistent with a previous report (Wyngaarden et al., 2010) and suggests that fin-field cells converge along the AP axis to become positioned within the fin bud.

We found that the relative AP positions of the cardiac, fin and peritoneum fields in the LPM are maintained after tissue differentiation from each precursor pool. Next, we asked whether the cells of the fin-field also exhibit a topological arrangement; that is, are relative AP positions of the cells maintained during convergence or does extensive mixing occur? We compared the initial AP position of labeled LPM cells in the fin-field with the averaged position of each resulting clone in the fin bud. This analysis revealed a correlation (Fig. S4B; $P<2.2\times10^{-16}$, $n$=72),

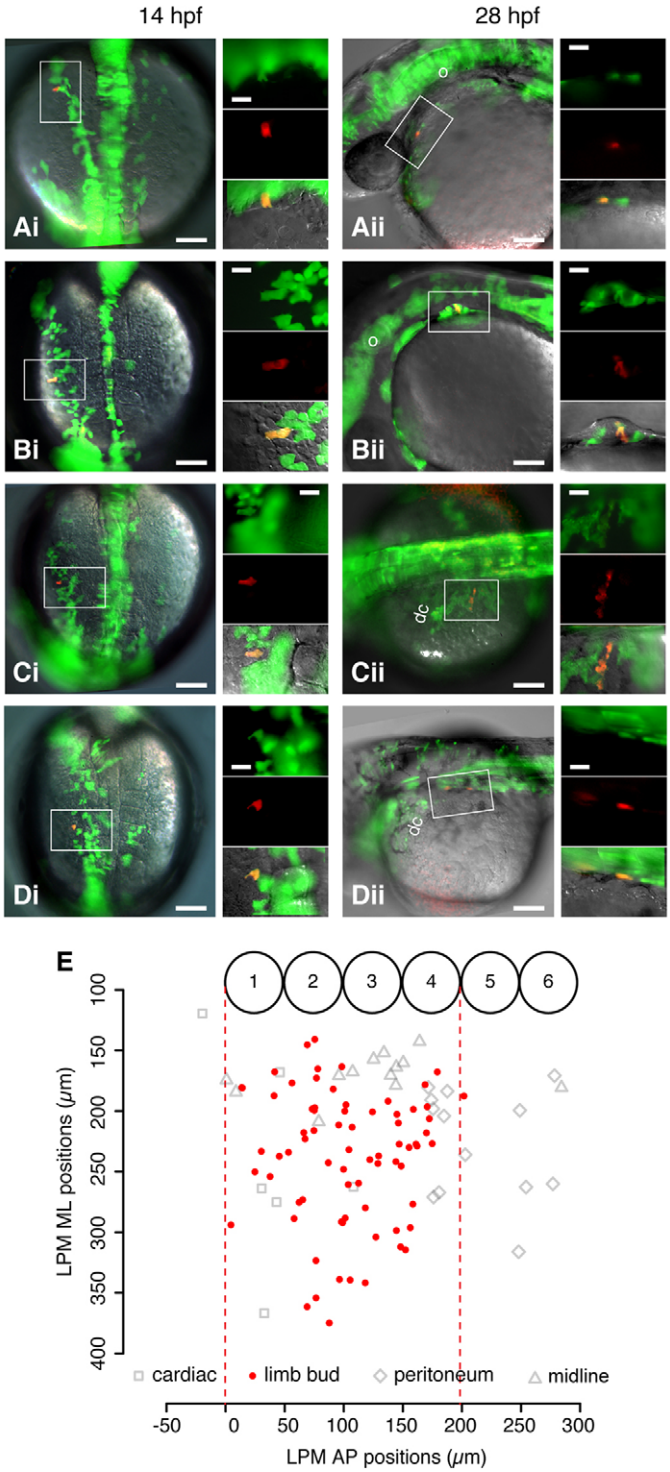


**Fig. 1. A single-cell-resolution fate map of the pectoral fin-field in the zebrafish LPM.** (Ai) Dorsal view of 14 hpf embryo previously injected with *Kaede* RNA in a single blastomere. Box shows a single cell photo-converted to express red fluorescence. Insets show the boxed region at higher magnification of green *Kaede* fluorescence (upper), red photo-converted cell (middle) and overlaid fluorescence with differential interference contrast microscopy (bottom). (Aii) Same embryo in lateral view at 28 hpf. Box shows resultant clone in cardiac region; insets are as in Ai. (Bi,Bii) Fin bud clone. (Ci,Cii) Peritoneum clone. (Di,Dii) Midline clone. Scale bars: 100 µm in overviews; 10 µm in insets. (E) Fate map of LPM cell fates at 14 hpf. *x*-axis: AP position relative to somite borders. *y*-axis: ML position from midline of embryo. Numbered circles denote somite positions. Red dashed lines delineate the fin-field at 14 hpf. dc, duct of Cuvier; ML, mediolateral; o, otic vesicle.

Development (2015) 142, 4329-4339 doi:10.1242/dev.124750

indicating a topological transfer of the anteroposterior arrangement of cells from the LPM fin-field at 14 hpf to the fin bud at 28 hpf.

### Fin-field cells converge topologically along the AP axis during pectoral fin bud initiation

In order to characterize the spatial dynamics of fin-field cells further, we used a transgenic line *Et(hand2:eGFP)ch2*, in which all LPM cells are marked with GFP (Fig. 2Ai-Di; Fig. S1; supplementary materials and methods) allowing three-dimensional cell tracking (Fig. 2Ai′-Di′; Fig. S2A-D; supplementary materials and methods). The transformation from the fin-field to the fin bud involves movements of ∼120 fin-field cells on each side of the embryo from 18 (onset of AP convergence) to 28 hpf (condensation of fin bud primordia). We tracked 60 cells unilaterally from somite levels 1-5+ in each of eight wild-type embryos from 18 to 23 hpf, when most fin-field LPM cell movements take place (Fig. S2E). Fig. 2Ai-Di′ and Movie 1 show time-lapse images in a double transgenic but otherwise wild-type embryo, in which *Et(hand2:eGFP)ch2* labels all LPM cells and *Tg(h2afx:h2afv-mCherry)mw3* labels all nuclei (McMahon et al., 2009). Registered cell tracks from eight wild-type embryos are collectively shown in Fig. 3Ai, with the origin of the axes at the intersection between the midline of the embryo and the anterior border of somite 1. Clustering these cell tracks into five color-coded groups corresponding to the inter-somitic borders flanking the track origins, we observed a general trend of caudally and laterally oriented net motility relative to the body axis (Fig. 3Ai). Subtraction of the averaged cell tracks of each LPM group from the averaged track of all LPM cells further revealed a net convergence of track groups 1-4,

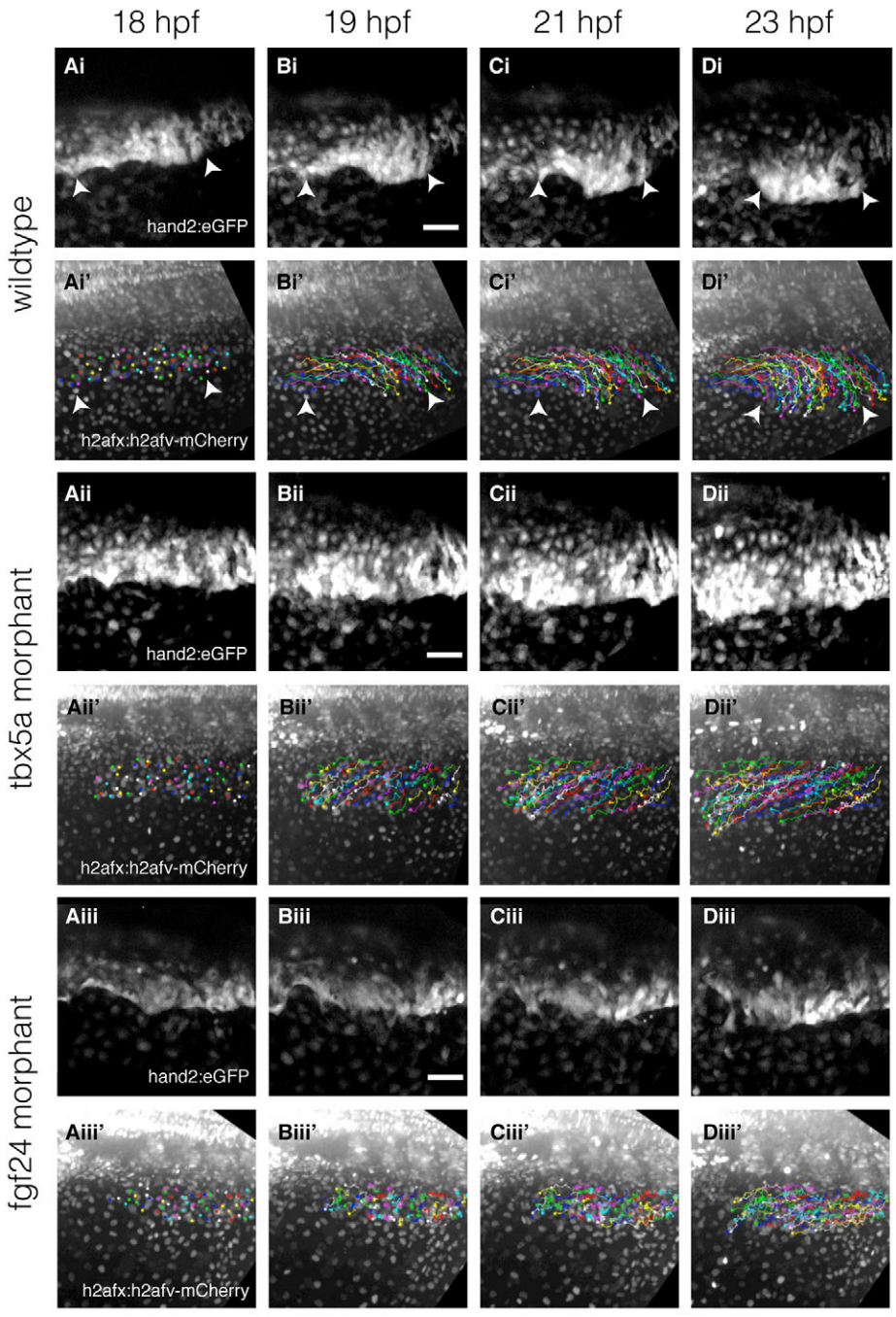


**Fig. 2. Time-lapse and cell tracking of the fin-field LPM during pectoral fin bud initiation in wild-type embryos and Tbx5a and Fgf24 morphants.** (Ai-Diii′) Time-lapse of double transgenic *Et(hand2:eGFP)ch2*; *Tg(h2afx:h2afv-mCherry)mw3* embryos with backgrounds of wild-type embryos (Ai-Di′), Tbx5a morphant (Aii- Dii′) and Fgf24 morphant (Aiii-Diii′). (Ai-Di,Aii-Dii,Aiii-Diii) Time-lapse stills showing convergence over time of eGFP-expressing fin-field cells. (Ai′-Di′,Aii′-Dii′,Aiii′-Diii′) Corresponding stills of mCherry-labeled nuclei overlaid with cell trajectories indexed by random colors. Dorsal view, anterior left. Scale bars: 50 µm. Arrowheads in Ai′-Di′ highlight the extent of the fin-field.

Development (2015) 142, 4329-4339 doi:10.1242/dev.124750

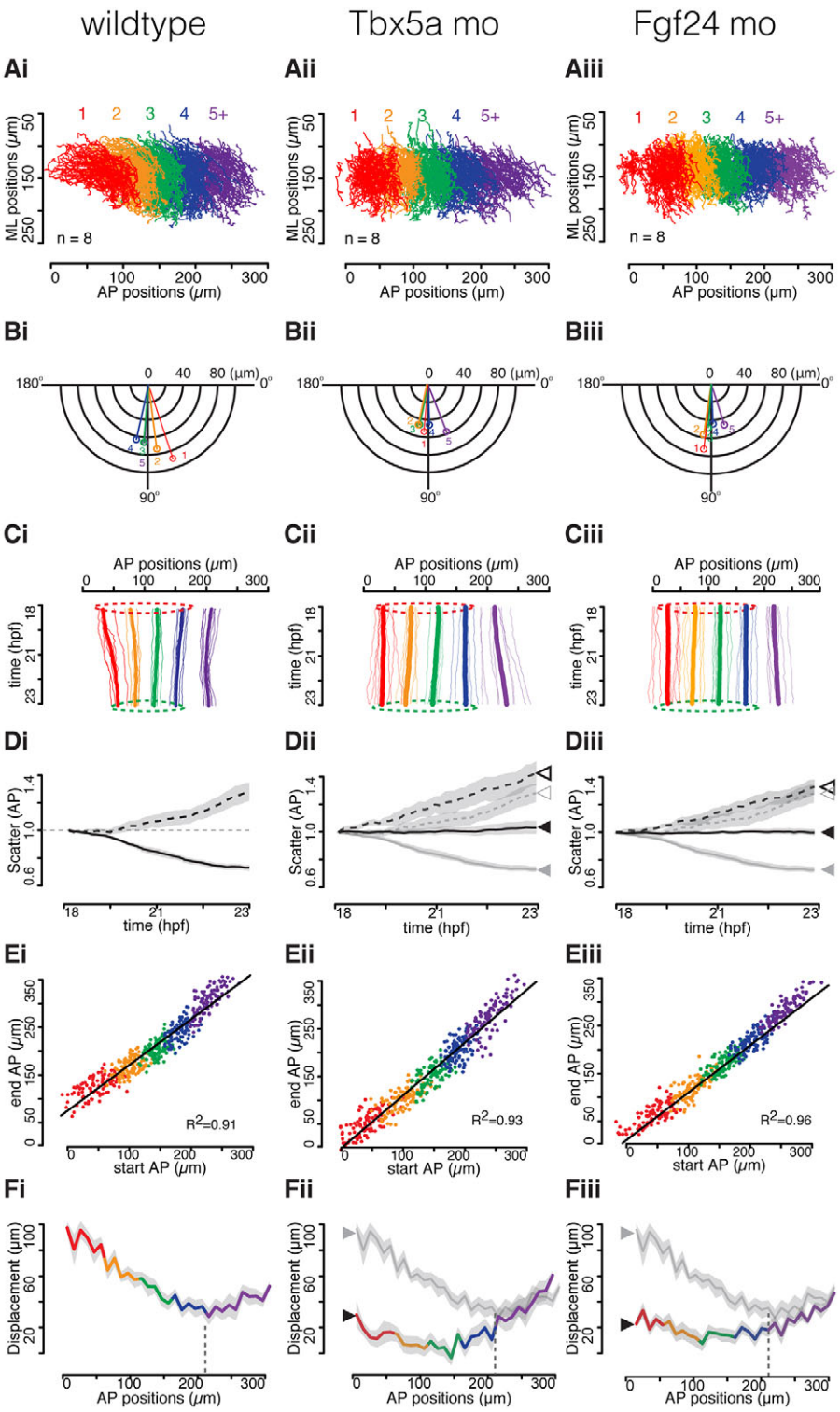


**Fig. 3. Quantitative analyses of cell tracks of the fin-field LPM during pectoral fin bud initiation in wild-type embryos and Tbx5a and Fgf24 morphants.** (Ai-Fiii) Each row shows identical quantification from eight embryos of the wild-type (Ai-Fi), Tbx5a morphant (Aii-Fii) and Fgf24 (Aiii-Fiii) background. (Ai-Aiii) Composite cell tracks, in which the color-coded groups, red, orange, green, blue and purple, represent LPM cells from somite levels 1, 2, 3, 4 and 5+, respectively. This color code is the same throughout all subsequent panels. (Bi-Biii) Polar plot showing the net average orientation and magnitude of displacement of the five track groups. (Ci-Ciii) Average net AP trajectories of the five track groups, subtracting the average AP trajectories of all LPM track groups. Fine lines represent group average from individual embryos; bold lines represent composite average from each group. Dotted circles denote average AP extent of fin-field domains at 18 (red) and 23 hpf (green). (Di-Diii) Scatter value along the AP axis by time. Dashed lines indicate the peritoneum field group. Solid lines indicate the fin-field group. Lines represent eight-embryo average; shaded areas represent 95% confidence interval. In Dii and Diii, open arrowheads show scatter of track group 5+ and solid arrowheads show scatter of track groups 1-4. Black shows value of morphant, whereas gray shows value of wild type (reproduced from Di). (Ei-Eiii) Correlation of starting AP positions with ending AP positions of tracked LPM cells. Solid line represents a linear least-squares regression of all data points; $r^2$ is the coefficient of determination. (Fi-Fiii) AP displacement value for individual track groups. Dashed vertical line represents the rough boundary at somite 4-5 between the fin-field and the peritoneum field. Solid lines represent eight-embryo average; shaded areas represent 95% confidence interval. In Fii and Fiii, black arrowhead shows value of morphant, whereas gray shows value of wild type (reproduced from Fi).

which separates them from the more posteriorly located track group 5 + (Fig. 3Bi,Ci). In order to identify and distinguish the converging and non-converging cell groups quantitatively, we defined the measurement ‘scatter’ to describe the variation of individual AP positions within a delineated group of cells (supplementary materials and methods). An increasing or decreasing scatter value over time indicates cell dispersion or convergence, respectively. A sliding maximal detection limit along the AP axis allowed us to identify the lowest scatter value point to define the border between converging and the non-converging LPM cell groups; this point roughly aligns with the border between track groups 4 and 5 (Fig. S2F,G), in agreement with the posterior limit of the fin-field revealed by our fate map (Fig. 1E). Henceforth, we refer to the definitive ‘fin-field’ as those LPM cells originating between somites 1 and 4 along the body axis of the 14 hpf zebrafish embryo, with the peritoneum field residing in more posterior LPM regions. As shown in Fig. 3Di, fin-field cells converge along the AP axis, in contrast to adjacent peritoneum progenitors that disperse over time.

Development (2015) 142, 4329-4339 doi:10.1242/dev.124750

A tight correlation exists between the starting and ending AP positions of individual cell tracks (Fig. 3Ei), attesting to the preservation of relative AP positions between fin-field cells and their progeny in the fin bud. Together, the fate map and cell-tracking data reveal that the pectoral fin-field initially occupies a broader area along the primary body axis than the final AP dimensions of the fin bud. The LPM fin-field cells then converge topologically to form the fin bud mesenchyme.

### A cell motility gradient along the AP axis underlies asymmetric fin-field convergence

The most anterior groups of LPM cells, initially residing next to somites 1 and 2 ('anterior fin-field'; Fig. 3Ai,Bi, red and orange groups; Fig. 3Fi, AP positions <100 µm), migrate further relative to those at more posterior initial locations next to somites 3 and 4 ('posterior fin-field'; Fig. 3Ai,Bi, blue and green groups; Fig. 3Fi, AP positions ~100-200 µm), resulting in an anterior-to-posterior gradient in displacement (Fig. 3Fi). The displacement measure can be affected by two factors, namely speed and persistence of motion in a given direction. After subtraction of the overall LPM tissue movement, anterior fin-field cells migrate at higher average speeds along the AP axis (Fig. S3A) and exhibit elevated persistence (the ratio of displacement to total trajectory length; supplementary materials and methods; Fig. S3B) and mean square displacement (MSD) values (Fig. S3F), relative to posterior fin-field cell groups. The elevated levels of net directional migration of anterior fin-field cells in the anterior-to-posterior direction relative to those of posterior fin-field cells in the posterior-to-anterior direction results in a convergence point positioned within the posterior fin-field (center of mass at roughly 180 µm; Fig. 6L and supplementary materials and methods).

### Tbx5a is required for asymmetric fin-field cell convergence

Tbx5 orthologs are required for forelimb bud formation in multiple vertebrates (Agarwal et al., 2003; Ahn et al., 2002; Garrity et al., 2002; Ng et al., 2002; Rallis et al., 2003; Takeuchi et al., 2003). Although we and others previously suggested the disruption of migration movements in Tbx5a-deficient embryos (Ahn et al., 2002; Garrity et al., 2002), it was not previously known how or when limb bud formation fails. In order to investigate the behavior of individual Tbx5a-deficient cells in the LPM further, we injected 1 ng Tbx5a antisense morpholino (a dose phenocopying the null Tbx5a mutant *heartstrings*) into *Et(hand2:eGFP)ch2*; *Tg(h2afx:h2afv-mCherry)mw3* embryos and performed live tracking analyses (Fig. 2Aii-Dii; Fig. S2H; Movie 2; $n$=60 tracks from each of eight embryos). Tbx5a-deficient fin-field cells fail to converge along the AP axis and migrate in near-parallel tracks laterally from the dorsal midline towards the ventral side of the body (Fig. 2Aii- Dii′; Fig. 3Aii-Cii). Notably, the caudalward migration of anterior fin-field cells observed in wild-type embryos (Fig. 3Bi,Ci,Fi) is diminished in magnitude in Tbx5a morphants, (Fig. 3Bii,Cii,Fii). The scatter value in the Tbx5a morphant fin-field remains constant over time, as opposed to the decreasing value for wild-type fin-field cells as they converge (Fig. 3Dii, black versus gray solid arrowhead). Furthermore, the descending gradients in displacement (Fig. 3Fii, black arrowhead compared with gray arrowhead), average speed, persistence and MSD (Fig. S3A,B,F, second column compared with first column) along the AP axis are diminished in the Tbx5a-deficient fin-field. Collectively, these data demonstrate that fin-field LPM cells, although still able to migrate, fail to converge along the AP axis in Tbx5a morphants. These LPM cells eventually scatter over the yolk and adopt a peritoneum-like morphology.

Interestingly, although cell convergence fails, Tbx5a-deficient fin-field cells maintain their topological migration pattern (Fig. 3Eii). Given that in the peritoneum field, where Tbx5a expression is normally absent, LPM cells also exhibit topological migration (Fig. 3Ei, purple dots), we hypothesize that the maintenance of nearest neighbor relationships during migration might be an intrinsic property of all LPM cells independent of Tbx5a function.

### Fgf24 functions as a posterior convergence cue for fin-field LPM cells

Given that Tbx5a is expressed throughout the AP length of the fin-field (Fig. 4A-D), its expression alone cannot account for the asymmetry in fin-field cell motility. Rather, Tbx5a might regulate a convergence cue located within the posterior half of the fin-field. One candidate is *fgf24*, a Tbx5a target that is required for the coalescence of Tbx5a$^+$ cells and formation of the pectoral fin (Draper et al., 2003; Fischer et al., 2003; Mercader et al., 2006). *fgf24* is expressed in a more restricted domain within the posterior position in the *tbx5a*$^+$ LPM (Fischer et al., 2003), roughly aligned with the future position of the prospective fin bud (Fig. 4E-H; note that the somitic landmarks have shifted posteriorly by one somite compared with 14 hpf).

To investigate whether Fgf24 is required as a convergence cue for fin-field LPM cells, we injected 1 ng of Fgf24 antisense morpholino into *Et(hand2:eGFP)ch2*; *Tg(h2afx:h2afv-mCherry)mw3* embryos and performed live cell tracking (Fig. 3Aiii-Diii; Fig. S2I; Movie 3;

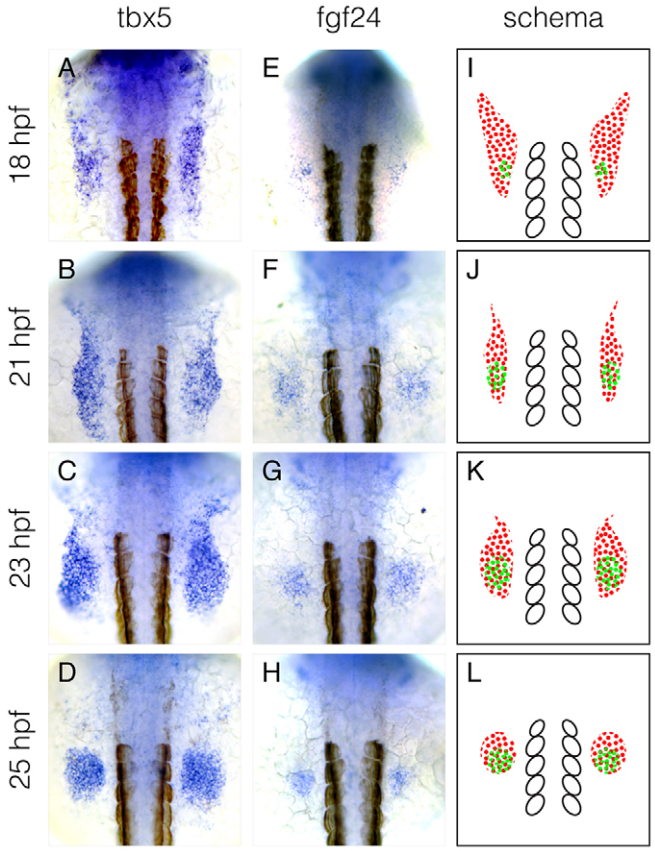


**Fig. 4. The mRNA expression pattern of *fgf24* overlaps with the posterior domain of *tbx5a* expression.** (A-H) mRNA expression pattern of *tbx5a* (A-D) and *fgf24* (E-H) at 18, 21, 23 and 25 hpf. (I-L) Schematics of mRNA expression patterns of *tbx5a* (red dots) and *fgf24* (green dots), highlighting the overlap between *tbx5a* and *fgf24* mRNA expression at the posterior limb-field. White ovals denote somites 1-5. Dorsal view, anterior up.

Development (2015) 142, 4329-4339 doi:10.1242/dev.124750

*n*=60 tracks from each of eight embryos). Fgf24 morphant cell motility along the AP axis essentially phenocopies that of the Tbx5a morphants; fin-field cells no longer converge along the AP axis (Fig. 3Aiii-Ciii) and instead migrate in parallel with a near-constant scatter value (Fig. 3Diii, solid black compared with solid gray arrowhead) and diminished displacement (Fig. 3Fiii, black compared with gray arrowhead), average speed, persistence and MSD along the AP axis (Fig. S3A,B,F, third compared with first and second columns). As in wild-type embryos and Tbx5a morphants, the topological relationship of LPM cells is maintained in Fgf24 morphant fin-fields (Fig. 3Eiii).

### Fin-field LPM cells in Fgf24 morphants can converge towards an ectopic Fgf source

Fgf24 expression is temporally and spatially correlated with its potential role as a convergence cue and is functionally required in fin bud initiation (Fig. 4; Fischer et al., 2003). To test whether fin-field LPM cells can migrate towards a localized Fgf source, we implanted polystyrene beads coated with recombinant human-mouse Fgf8b (a paralog of Fgf24; Jovelin et al., 2007) into the fin-field LPM in Fgf24 morphants and performed cell tracking (*n*=20 cells in each of eight embryos; Fig. 5; Fig. S5; Movie 4A,B).

We found that Fgf8b-coated beads can induce a convergence-like movement of fin-field LPM cells (Fig. 5E-H; Movie 4B; Fig. S5I-P) compared with bovine serum albumin (BSA)-coated control beads (Fig. 5A-D; Movie 4A; Fig. S5A-H), as indicated by the declining average distances between tracked cells and beads (Fig. 5I, orange compared with blue line). The presence of an Fgf8b-coated bead alters nearby fin-field cell behaviors in Fgf24 morphants, such that these cells migrate with higher speed (Fig. 5J; Wilcoxon test $P=7.3\times10^{-16}$) and persistence (Fig. 5K; Wilcoxon test $P=2.8\times10^{-15}$) compared with those adjacent to control BSA-coated beads.

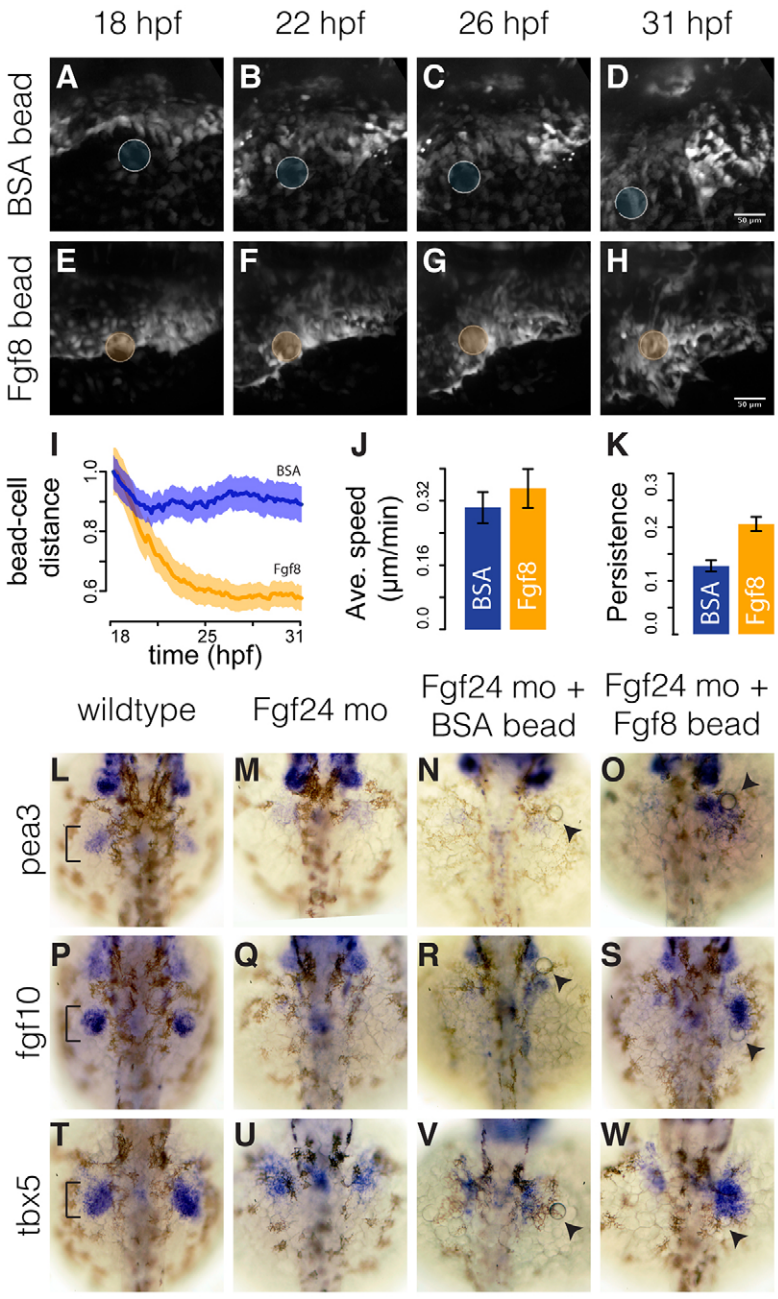


**Fig. 5. Fin-field LPM cells in Fgf24 morphants can converge towards Fgf8b-coated beads.** (A-H) Stills from time-lapse of Fgf24 morphant embryos implanted with either a BSA-coated bead (A-D) or an Fgf8b-coated bead (E-H). Scale bars: 50 μm. (I) Temporal progression of relative distances of tracked cells to implanted BSA- or Fgf8b-coated beads. Solid lines show eight-embryo average. Shaded areas show eight-embryo 95% confidence interval. *n*=20 tracks per embryo. (J,K) Average speed (J) and persistence (K) of tracked cells in Fgf24 morphant embryos with BSA- or Fgf8b-coated beads. Error bars show eight-embryo 95% confidence interval. (L-W) Dorsal views of fin bud region (brackets) in 36 hpf embryos showing *pea3* (L-O), *fgf10* (P-S) and *tbx5a* (T-W) expression in wild types, Fgf24 morphants, Fgf24 morphants with a BSA-coated bead and Fgf24 morphants with an Fgf8b-coated bead. Arrowheads point to implanted beads.

Development (2015) 142, 4329-4339 doi:10.1242/dev.124750

Fgf24 loss of function perturbs the activation of *pea3* (*etv4* – Zebrafish Information Network) and *fgf10* and the maintenance of *tbx5a* in the fin initiation gene network (Fischer et al., 2003; Fig. 5M,Q,U compared with Fig. 5 L,P,T). Although control beads failed to rescue expression of *pea3*, *fgf10* and *tbx5a* in the fin-field (Fig. 5N,R,V), Fgf8b-coated beads induced their expression around the implantation sites within the fin-field (Fig. 5O,S,W). This suggests that ectopic Fgf8, when introduced in a comparable spatiotemporal pattern to endogenous Fgf24, can rescue aspects of the fin initiation gene network in Fgf24 morphants. Taken together, these results demonstrate that fin-field LPM cells can migrate towards a localized Fgf source in a chemoattractive fashion during fin initiation.

### Reduction in Tbx5a or Fgf24 levels results in biased disruption of fin-field cell convergence and unequal truncations in the fin AP axis

We have previously shown that suboptimal doses of Tbx5a morpholino can reduce the size of larval pectoral fins and cause tissue gaps preferentially on the anterior side of the endoskeletal disc (Ahn et al., 2002; Fig. 6B, asterisks). The anteriorly biased truncations are reminiscent of the pre-axial hemimelia observed in *TBX5*-haploinsufficient individuals with Holt–Oram syndrome (Basson et al., 1997; Brassington et al., 2003; Li et al., 1997). The intrinsic asymmetry in fin-field cell convergence pattern led us to hypothesize that partial reduction in Tbx5a or Fgf24 levels might have differential effects upon anterior versus posterior subpopulations within the fin-field.

To test whether the AP axis in the fin bud of Tbx5a or Fgf24 partial morphant embryos is disrupted, we injected *Et(hand2:eGFP)ch2*; *Tg(h2afx:h2afv-mCherry)mw3* embryos with suboptimal doses of Tbx5a or Fgf24 morpholino (0.6 ng for Tbx5a, 0.4 ng for Fgf24; Fig. S2J,K; $n$=60 tracks in each of eight embryos per treatment). Tbx5a or Fgf24 partial morphant fin-field cells display an overall intermediate level of AP convergence (Fig. 6C,D; Fig. S6C,D; black solid arrowhead in Fig. 6E or Fig. S6E) and displacement gradient (black arrowhead in Fig. 6K or Fig. S6K) compared with wild-type embryos and Tbx5a or Fgf24 full morphants. The average speed, persistence and MSD of the anterior fin-field cells in partial Tbx5a or Fgf24 morphants more closely resemble those of Tbx5a or Fgf24 full morphants rather than wild-type embryos (Fig. S3A,B,F,G). We further quantified the proportions (relative to the total number initially present) of anterior or posterior fin-field cells that successfully became incorporated into the fin bud (Fig. 6L,M; Fig. S6L,M; supplementary materials and methods). In Tbx5a partial morphants, only 18% of anterior fin-field cells contributed to the fin bud, compared with a 47% incorporation rate of posterior fin-field cells (Fig. 6M; Wilcoxon test $P$=0.0027). Therefore, whereas cell migration across the entire fin-field is affected in partial Tbx5a morphants, the anterior population is more affected by decreased Tbx5a levels. A similar conclusion can be drawn with Fgf24 partial morphants (Fig. S6M; Wilcoxon test $P$=0.028).

To test whether the differential convergence defects between anterior versus posterior fin-fields observed in partial morphants are correlated with later patterning defects, we quantified the areas occupied by *hoxc6a*$^+$ or *hoxd12a*$^+$ cells, which mark the anterior and posterior fin bud mesenchyme, respectively (Fig. 6F,G; Gibert et al., 2006; Molven et al., 1990; Neumann et al., 1999). The expression domains of *hoxc6a* and *hoxd12a* are both reduced in Tbx5a or Fgf24 partial morphants (Fig. 6H,I; Fig. S6H,I) in comparison to wild-type embryos (Fig. 6F,G; Fig. S6F,G); however, the *hoxc6a* expression domain is reduced ∼40% more than that of *hoxd12a* (Fig. 6J, Tbx5a partial morphants; Fig. S6J, Fgf24 partial morphants).

Together, these results suggest that partial reduction in Tbx5a or Fgf24 levels results in preferential disruption of anterior fate in the early fin bud. Given that this is correlated with a greater reduction in the convergence of the anterior subpopulation of fin-field cells, we propose that an early mechanism might pre-pattern the vertebrate fin AP axis prior to or during the fin-field convergence. We propose that a greater sensitivity to the levels of Tbx5a or Fgf expression in anterior fin-field cells versus posterior fin-field cells could contribute to the anteriorly biased defects observed in individuals with Holt–Oram syndrome.

## DISCUSSION

### Tbx5a orchestrates a topological and asymmetric LPM cell migration underlying limb initiation

A quantitative model of how early LPM cells become organized prior to limb bud formation, especially with regard to cell migration, does not exist for any vertebrate embryo. Here, we have characterized the dynamics of LPM migration to form the fin bud by combining a single-cell-resolution fate map with live cell tracking. We established that the definitive fin-field occupies the area of the zebrafish LPM adjacent to somites 1-4. This broad extent of the fin-field, relative to the initial fin bud, which only covers the area between somites 2 and 3, suggests that LPM cells must migrate and converge to form the fin bud proper. Time-lapse analyses confirm that convergence movements of the fin-field LPM supply the majority of the mesenchymal complement of the early fin bud. Migration movements of the LPM fin-field cells are coordinated and coherent, maintaining a topological relationship between the initial AP organization of the LPM along the body axis with the final AP location of these cells within the forming fin bud.

Our studies show that fin-field cells do not simply converge symmetrically towards a center point, contrary to what had been proposed by previous studies using somites as landmarks (Ahn et al., 2002; Wyngaarden et al., 2010). In zebrafish, the LPM and somites are known to shift relative to one another at this stage (Devoto et al., 1996). By tracking the movements of individual cells within the fin-field, we have shown that a cell motility gradient along the AP axis results in the final position of the fin bud being located posteriorly within the fin-field. We hypothesize that the differential fin-field cell movements indicate either a pre-patterning of different movement characteristics or an active migration towards an asymmetrically localized signaling center. Together, these data define a model in which asymmetric but topological cell convergence transforms the initially broad LPM fin-field into the compact early fin bud.

The overall extent and subsequent shape changes of the fin-field closely mirror the dynamic expression pattern of zebrafish *tbx5a* gene during development (Fig. 4A-D). Previously, it was shown that Tbx5a deficiency causes a complete loss of pectoral fins (Ahn et al., 2002; Garrity et al., 2002). Here, we show that loss of Tbx5a function abolishes the differences both in distance and in angle of migration amongst the different groups of fin-field cells. As a result, fin-field cells migrate along parallel tracks relative to each other along the dorsoventral embryonic axis and display little to no relative movement in the AP direction. Therefore, loss of Tbx5*a* does not affect the ability of the cells to migrate per se, but does affect their ability to track collectively towards a convergence target area.

Development (2015) 142, 4329-4339 doi:10.1242/dev.124750

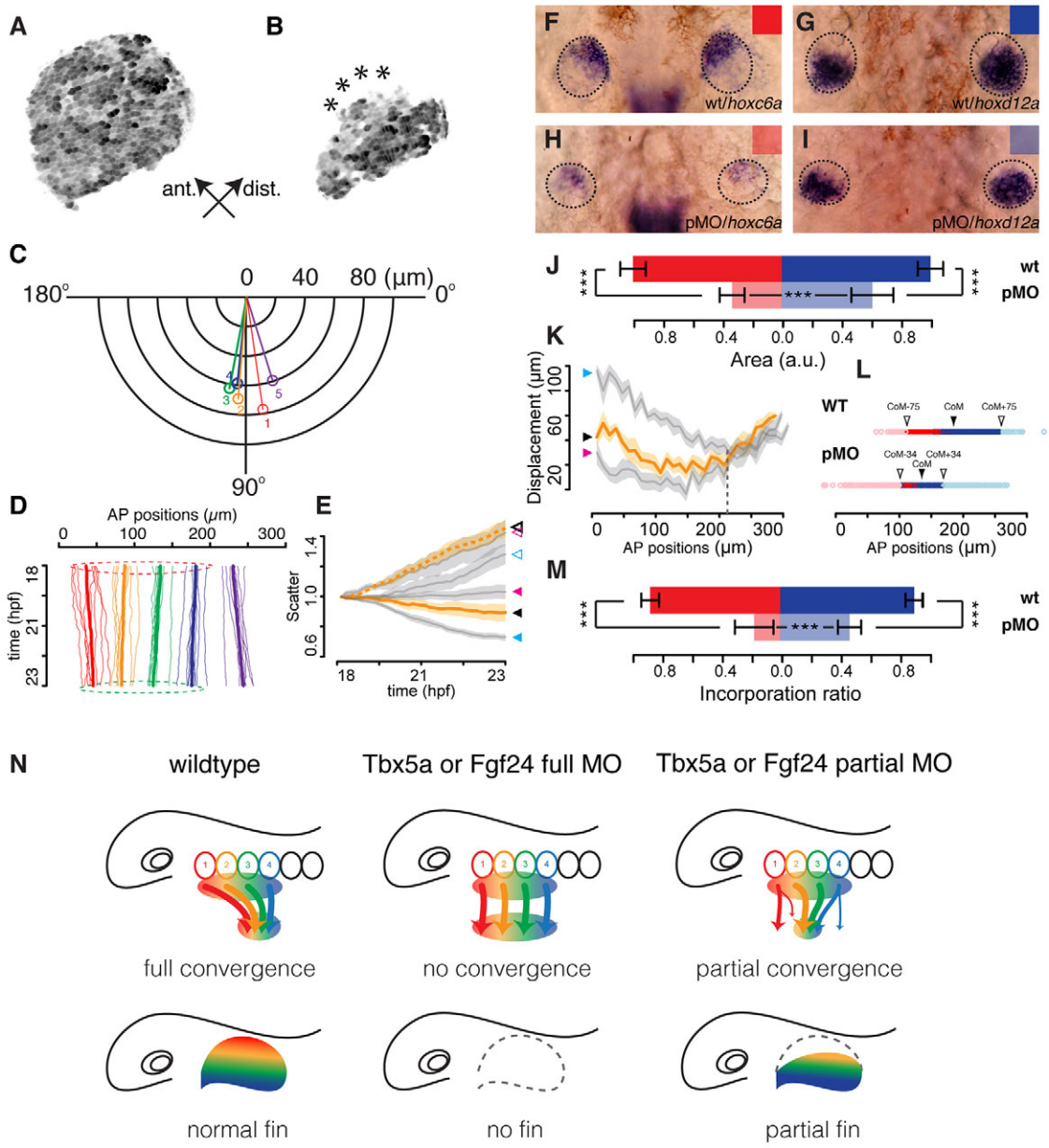


**Fig. 6. Incomplete cell convergence in the fin-field of Tbx5a partial morphants is correlated with anteriorly biased truncations in fin buds.** (A,B) Maximal intensity projections of the pectoral cartilaginous disc in 4 dpf *Tg(b-act2:Brainbow1.0L)*$^{pd49}$ larvae of an otherwise wild-type embryo (A) and a Tbx5a partial morphant (B); asterisks highlight lesions on the anterior edge of the cartilaginous disc. (C) Polar plot showing net average orientation and magnitude of displacement of the five track groups in eight Tbx5a partial morphant embryos. (D) Average net AP trajectories of five track groups relative to the overall trajectories in all LPM tracks in eight Tbx5a partial morphant embryos. Dashed circles highlight the similar AP extent of fin-field domains between 18 (red) and 23 hpf (green). (E) Scatter values in eight wild-type embryos (blue arrowhead), eight Tbx5a full morphants (pink arrowhead) and eight Tbx5a partial morphants (black arrowhead). Solid arrowhead represents fin-field; open arrowhead represents peritoneum field. Lines represent eight-embryo average; shaded areas represent 95% confidence interval. (F-I) Expression patterns of *hoxc6a* (F,H) and *hoxd12a* (G,I) in the 36 hpf fin buds of wild-type (wt; F,G) and Tbx5a partial morphant (pMO) embryos (H,I; dorsal view, anterior up). (J) Quantification of expression areas of *hoxc6a* (red) and *hoxd12a* (blue) in wild-type embryos (dark color) and Tbx5a partial morphants (light color; *n*=40 each). (K) AP displacement plotted against starting AP positions in eight wild-type embryos (blue arrowhead), eight Tbx5a full morphants (red arrowhead) and eight Tbx5a partial morphants (black arrowhead). Dashed vertical line represents the rough boundary at somite 4-5 between the fin and peritoneum fields. Solid lines represent eight-embryo average; shaded areas represent eight-embryo 95% confidence interval. (L) Track ending AP positions of fin-field tracks in eight wild-type embryos (WT) and eight Tbx5a partial morphants (pMO). CoM, center of mass; CoM-75/CoM+75, anterior/posterior limits of the wild-type fin bud; CoM-34/CoM+34, anterior/posterior limits of the Tbx5a partial morphant fin bud. (M) Quantification of incorporation ratio of anterior (red, somites 1-2) and posterior (blue, somites 3-4) fin-field tracks in wild-type embryos (dark color) and Tbx5a partial morphants (light color; *n*=40 each). Wilcoxon test: ***$P$=9.1×10$^{-4}$ (A tracks wild type-Tbx5a pMO); ***$P$=1.6×10$^{-4}$ (P tracks wild type-Tbx5a pMO); ***$P$=2.7×10$^{-3}$ (A tracks Tbx5a pMO-P tracks Tbx5a pMO). (N) Models of fin bud initiation in various conditions. First column: in wild types, fin-field cells undergo asymmetric and topological AP convergence. Fin-field positional information (rainbow color) translates into AP axis patterning in the fin. Second column: in Tbx5a or Fgf24 full morphants, all fin-field cells fail to converge, resulting in initiation failure and absence of fins. Third column: in Tbx5a or Fgf24 partial morphants, some fin-field cells fail to converge, with anterior fin-field cells preferentially mis-migrating. Given that positional information might be specified in the early fin-field, reduced incorporation of anterior progenitors results in the anteriorly biased truncation of the fin.

Development (2015) 142, 4329-4339 doi:10.1242/dev.124750

### Role of Fgf signaling during fin-field convergence and fin bud initiation

Although the importance of cell migration in limb bud formation is increasingly acknowledged, much less is known about the genetic and molecular functions of signals within the converging pre-limb bud mesenchyme. Several Fgfs are expressed in the intermediate and lateral plate mesoderm preceding formation of the limb bud. We and others (Gros and Tabin, 2014) hypothesize that mesenchymal Fgf signals play a key role in the transition from limb/fin-field to limb/fin bud. Fgf24 is a teleost-specific member of the *fgf8/fgf17/18* family (Jovelin et al., 2007) and is the earliest Fgf member to be expressed in the fin-field region. Previously, knockdown of Fgf24 was shown to cause absence of pectoral fins, similar to Tbx5a deficiency (Draper et al., 2003; Fischer et al., 2003). Fgf24 is a known target of Tbx5a (Fisher et al., 2003). Here, we show that disruptions in LPM cell migrations are similar in Fgf24- and Tbx5a-deficient specimens, with one notable difference. In Tbx5a-deficient embryos, the differences in both directionality and distance displayed by different wild-type AP populations of fin-field cells are lost (compare Fig. 3Bi with Bii). In Fgf24-deficient embryos, although AP convergence movements are similarly abrogated, the anterior population of fin-field cells still retains the ability to migrate further and faster than the posterior fin-field cells along the ML axis (Fig. 3Biii; Fig. S3C-E,I). This difference reveals that anterior fin-field cells might have an intrinsically higher motility that requires Tbx5a function but is independent of Fgf24 function.

At present, the mechanism that produces a restricted *fgf24* expression domain within a broader Tbx5 expression domain, despite Tbx5 being the only known activator, is not yet explained. Early signals, such as Wnt2b, which is required for expression of both *tbx5a* and *fgf24* (Fischer et al., 2003), could potentially introduce a bias in Fgf24 activation within the *tbx5a*$^{+}$ fin-field. Given that Wnt2b is expressed at an earlier time point in a restricted domain in the intermediate mesoderm immediately adjacent to the Tbx5$^{+}$ LPM, it is a potential candidate to fulfill the role of a local activator of *fgf24* expression; however, more in depth studies are warranted.

To test the hypothesis that Fgf24 acts as a non-cell-autonomous convergence cue to redirect the migration of anterior fin-field cells towards the posterior fin-field, we implanted beads coated with recombined Fgf8b into the fin-field of the zebrafish embryo. Although this approach did not elicit a full rescue of fin bud formation in Fgf24-deficient embryos, fin-field cells did reorient their migration pathways to converge upon the Fgf-coated beads. In chick embryos, Fgf-coated beads cause ectopic limb development, but the mechanism is controversial (Lewandoski et al., 2000; Moon and Capecchi, 2000). Recently, Fgf8-soaked beads placed into later-stage formed chick limb buds were shown to attract mesenchyme cells (Gros et al., 2010); however, this finding does not directly address a potential earlier role for Fgf as a chemoattractant within the tetrapod mesenchyme before limb bud formation. It has been postulated that an Fgf8 signal from the intermediate mesoderm could function as a limb inducer (Agarwal et al., 2003; Crossley et al., 1996; Moon and Capecchi, 2000; Vogel et al., 1996). Interestingly, conditional knockout of Fgf8 before the onset of expression in the apical ectodermal ridge reduces the size of the hindlimb bud in an apoptosis-independent manner (Sun et al., 2002). This suggests that a previously unsuspected Fgf mechanism might regulate the number of precursor cells that ultimately contribute to the limb bud. We speculate that an Fgf molecule might play a similar role in tetrapods as in zebrafish to induce cell convergence into the nascent limb bud position. Alternatively, as Fgf signaling has also been shown to promote cell motility locally in a non-directional manner (Bénazéraf et al., 2010; Gros et al., 2010), Fgfs might permissively promote cell motility in the limb-field, thus enabling limb-field cells to respond to an instructive signal such as Wnt5a, which has been shown to promote oriented cell behaviors during tetrapod limb bud development (Wyngaarden et al., 2010).

Preliminary studies (Q.M. and H.K.S., unpublished data) suggest that Tbx5a morphant fin-field cells do not appear to alter their migration direction, speed or persistence as robustly as Fgf24 morphant cells when presented with an Fgf8-coated bead. Although more studies are needed, these initial results suggest that, beyond inducing Fgf24 expression, Tbx5a might have additional roles in controlling fin-field LPM cell convergence. One possibility that we are currently investigating is whether Tbx5a is also required for the expression of an Fgf receptor (Fgfr) in the fin-field. If indeed the difference in fin-field responsiveness to an Fgf signal between Tbx5a and Fgf24 morphants is attributable to an Fgfr downstream to Tbx5a, we would hypothesize the existence of an Fgfr whose expression is directly regulated by Tbx5a but perhaps not by Fgf24.

### A fin-field pre-pattern might explain HOS-like phenotypes

We have demonstrated that partial reduction in Tbx5a or Fgf24 levels leads to an anteriorly biased perturbation of LPM cell convergence. Interestingly, loss of anterior cell migration often results in anteriorly distorted truncation of the AP axis in the pectoral fin cartilaginous disc, and this bias is also reflected in the expression of Hox (AP identity) genes. We suggest that the AP identity of fin-field cells (i.e. pre-pattern) might be specified early, preserved throughout the orderly fin-field cell convergence and eventually translated into the AP identity of the fin bud and fin skeleton. This can explain the correlated spatial bias between mis-migrating fin-field cells, reduction in fin bud fate markers, and skeletal defects in partial Tbx5a or Fgf24 morphants. It is possible that the pre-pattern can be shaped as early as gastrulation, when the LPM is exposed to multiple morphogen gradients, such as Retinoic acid along the AP axis (Keegan et al., 2005).

We propose that the pre-axial hemimelia displayed by individuals with Holt–Oram syndrome might be attributable in part to the preferential mis-migration of anterior limb-field cells during limb bud initiation. In multiple vertebrate species (mouse, chicken and zebrafish), the migration of LPM cells has now been shown to be involved during limb bud development (Wyngaarden et al., 2010). Here, we show that an early biased disruption in zebrafish fin-field cell convergence generates a distorted fin bud with proportionally fewer anterior fin progenitors than posterior ones. Interestingly, AP distortion in mouse limb bud fates by ectopic activation of Shh (Knezevic et al., 1997; Krawchuk et al., 2010; Zhang et al., 2010) recapitulates the pre-axial hemimelia condition observed in Holt–Oram syndrome. These findings argue that pre-axial hemimelia results from distortion of the AP axis, which can result from either early migration errors by fin-field cells or later patterning defects within the fin bud proper. Most importantly, our findings show that a balanced ratio of anterior to posterior fin progenitors is crucial for proper fin development. Given that many similar processes are involved in *de novo* development and in regeneration, we believe that the ratio of anterior versus posterior cells might be an important factor in the ability of a limb to regenerate. Finally, most congenital limb malformations possess a Mendelian underpinning in a defective developmental pathway (de Graaff and Kozin, 2009). We propose that our work provides a reference model for an examination of early cellular events during limb bud initiation in

Development (2015) 142, 4329-4339 doi:10.1242/dev.124750

other models of human diseases, which might shed light on common root causes of limb birth defects.

## MATERIALS AND METHODS

### Zebrafish embryos, morpholino injection and *in situ* hybridization

Embryonic and adult zebrafish were raised and maintained in standard laboratory conditions (Westerfield, 2007). *Et(hand2:eGFP)ch2* was generated with an eGFP-containing Tol2 transgenic construct (D. G. Ahn; supplementary materials and methods). *Tg(h2afx:h2afv-mCherry)mw3* was a gift from B. Link (McMahon et al., 2009). *Tg(b-act2:Brainbow1.0L)pd49* was provided by K. Poss (Gupta and Poss, 2012). Morpholino (Gene Tools, LLC) injections were performed as described by Nasevicius and Ekker (2000) (see supplementary materials and methods). Chromogenic mRNA *in situ* hybridizations were performed as described by Ahn et al. (2002) (see supplementary materials and methods). Quantification of gene expression area was performed by manual color thresholding with the RGB Threshold function in ImageJ (National Institutes of Health) for 100% incorporation of NBT/BCIP signals into the thresholded area.

### Fate map construction

A single marginal blastomere in the 64- or 128-cell-stage embryo was injected with 25 ng/µl *Kaede* mRNA. A single LPM cell from the labeled blastomere clone at 14 hpf was illuminated for 20-30 s through a pinhole in combination with a 63× dipping objective mounted on a Zeiss Axioplan microscope with light from a 100 W HBO mercury bulb passing through a DAPI filter set. Dorsal and lateral views of the embryos were photographed using a Nikon D5000 camera immediately after photo-conversion, at 28 and 48 hpf. The positions of the labeled progeny were analyzed further in ImageJ.

### Bead implantation

Bead implantation procedures followed those described by Picker et al. (2009) with the following modifications. Recombinant human-mouse Fgf8b protein (R&D Systems; cat. no. 423-F8-025) was diluted to 125 ng/µl in 0.1% BSA in 1× PBS and incubated with Polystyrene 45.0 µm microspheres (Polysciences; cat. no. 07314) overnight at 4°C. Embryos at 14 hpf were stabilized on 3% methylcellulose covered by Ringer solution before a mineral oil droplet was administrated through a micropipette to remove the epidermis over the targeted LPM region. A tungsten needle was used to position a loaded bead into the LPM. Embryos were then left undisturbed in E3 medium for at least 1 h before embedding into low-melting-point agarose for live imaging or fixing in 4% PFA for RNA *in situ* hybridization.

### Three-dimensional live imaging, cell tracking and statistical analysis

Live imaging of the fin-field was performed using *Et(hand2:eGFP)ch2*; *Tg(h2afx:h2afv-mCherry)mw3* double hemizygous embryos. Dechorionated embryos were mounted in 0.7% low-melting-point agarose (Sigma; A9414) in a glass-bottomed Petri dish containing E3 medium with 0.16% tricaine and kept at 27°C on a heated stage. *z*-stacks were collected every 8 min with a 20×/0.7 water-immersion objective on an inverted Olympus DSU spinning disk microscope. Cell tracking was performed semi-automatically. Maximal intensity projections were created from the mCherry channel *z*-stacks and were used for generating two-dimensional tracks. Sixty cell tracks were generated per embryo with the FIJI Manual Tracking plug-in by randomly selecting nuclei from one side of the LPM. Two-dimensional tracks were then imported into a custom FIJI macro to generate *z*-coordinates. Subsequent computational analyses were performed in R. Detailed tracking procedures and trajectory analyses are described further in the supplementary materials and methods. Wilcoxon rank sum test was performed as described by Bauer (1972).

#### Acknowledgements

We thank V. Bindokas and the EMBO 3D Developmental Imaging Course for microscopy support, Adam Kuuspalu for animal care and E. L. Ferguson and V. E. Prince for helpful comments on the manuscript. We thank D. G. Ahn for generating and providing the *Et(hand2:eGFP)ch2* enhancer trap line.

#### Competing interests

The authors declare no competing or financial interests.

#### Author contributions

Q.M. and R.K.H. conceived the initial project. Q.M. and H.K.S. performed the bead experiments. Q.M. performed fate-mapping and cell-tracking experiments and data analyses. Q.M., H.K.S. and R.K.H. wrote the manuscript.

#### Funding

This work is funded by a National Center for Research Resources and the National Center for Advancing Translational Sciences National Institutes of Health grant [UL1 RR024999], by a CBC scholarship from the Chicago Biomedical Consortium with support from The Searle Funds at The Chicago Community Trust to Q.M., a National Science Foundation Graduate Research Fellowship to H.K.S., and National Institutes of Health grant [HD072598 to R.K.H]. Deposited in PMC for release after 12 months.

#### Supplementary information

Supplementary information available online at
http://dev.biologists.org/lookup/suppl/doi:10.1242/dev.124750/-/DC1

#### References

**Agarwal, P., Wylie, J. N., Galceran, J., Arkhitko, O., Li, C., Deng, C., Grosschedl, R. and Bruneau, B. G.** (2003). Tbx5 is essential for forelimb bud initiation following patterning of the limb field in the mouse embryo. *Development* **130**, 623-633.

**Ahn, D.-G., Kourakis, M. J., Rohde, L. A., Silver, L. M. and Ho, R. K.** (2002). T-box gene tbx5 is essential for formation of the pectoral limb bud. *Nature* **417**, 754-758.

**Ando, R., Hama, H., Yamamoto-Hino, M., Mizuno, H. and Miyawaki, A.** (2002). An optical marker based on the UV-induced green-to-red photoconversion of a fluorescent protein. *Proc. Natl. Acad. Sci. USA* **99**, 12651-12656.

**Basson, C. T., Cowley, G. S., Solomon, S. D., Weissman, B., Poznanski, A. K., Traill, T. A., Seidman, J. G. and Seidman, C. E.** (1994). The clinical and genetic spectrum of the Holt-Oram syndrome (heart-hand syndrome). *N. Engl. J. Med.* **330**, 885-891.

**Basson, C. T., Bachinsky, D. R., Lin, R. C., Levi, T., Elkins, J. A., Soults, J., Grayzel, D., Kroumpouzou, E., Traill, T. A., Leblanc-Straceski, J. et al.** (1997). Mutations in human cause limb and cardiac malformation in Holt-Oram syndrome. *Nat. Genet.* **15**, 30-35.

**Bauer, D. F.** (1972). Constructing confidence sets using rank statistics. *J. Am. Stat. Assoc.* **67**, 687-690.

**Bénazéraf, B., Francois, P., Baker, R. E., Denans, N., Little, C. D. and Pourquié, O.** (2010). A random cell motility gradient downstream of FGF controls elongation of an amniote embryo. *Nature* **466**, 248-252.

**Bénazet, J.-D., Bischofberger, M., Tiecke, E., Gonçalves, A., Martin, J. F., Zuniga, A., Naef, F. and Zeller, R.** (2009). A self-regulatory system of interlinked signaling feedback loops controls mouse limb patterning. *Science* **323**, 1050-1053.

**Boulet, A. M., Moon, A. M., Arenkiel, B. R. and Capecchi, M. R.** (2004). The roles of Fgf4 and Fgf8 in limb bud initiation and outgrowth. *Dev. Biol.* **273**, 361-372.

**Brassington, A.-M. E., Sung, S. S., Toydemir, R. M., Le, T., Roeder, A. D., Rutherford, A. E., Whitby, F. G., Jorde, L. B. and Bamshad, M. J.** (2003). Expressivity of Holt-Oram syndrome is not predicted by TBX5 genotype. *Am. J. Hum. Genet.* **73**, 74-85.

**Crossley, P. H., Minowada, G., MacArthur, C. A. and Martin, G. R.** (1996). Roles for FGF8 in the induction, initiation, and maintenance of chick limb development. *Cell* **84**, 127-136.

**Damon, B. J., Mezentseva, N. V., Kumaratilake, J. S., Forgacs, G. and Newman, S. A.** (2008). Limb bud and flank mesoderm have distinct “physical phenotypes” that may contribute to limb budding. *Dev. Biol.* **321**, 319-330.

**de Graaff, E. and Kozin, S. H.** (2009). Genetics of radial deficiencies. *J. Bone Joint Surg.* **91** Suppl. 4, 81-86.

**Devoto, S. H., Melançon, E., Eisen, J. S. and Westerfield, M.** (1996). Identification of separate slow and fast muscle precursor cells in vivo, prior to somite formation. *Development* **122**, 3371-3380.

**Draper, B. W., Stock, D. W. and Kimmel, C. B.** (2003). Zebrafish fgf24 functions with fgf8 to promote posterior mesodermal development. *Development* **130**, 4639-4654.

**Fischer, S., Draper, B. W. and Neumann, C. J.** (2003). The zebrafish fgf24 mutant identifies an additional level of Fgf signaling involved in vertebrate forelimb initiation. *Development* **130**, 3515-3524.

**Foty, R. A., Pfleger, C. M., Forgacs, G. and Steinberg, M. S.** (1996). Surface tensions of embryonic tissues predict their mutual envelopment behavior. *Development* **122**, 1611-1620.

**Garrity, D. M., Childs, S. and Fishman, M. C.** (2002). The heartstrings mutation in zebrafish causes heart/fin Tbx5 deficiency syndrome. *Development* **129**, 4635-4645.

**Gibert, Y., Gajewski, A., Meyer, A. and Begemann, G.** (2006). Induction and prepatterning of the zebrafish pectoral fin bud requires axial retinoic acid signaling. *Development* **133**, 2649-2659.
**Gros, J. and Tabin, C. J.** (2014). Vertebrate limb bud formation is initiated by localized epithelial-to-mesenchymal transition. *Science* **343**, 1253-1256.
**Gros, J., Hu, J. K.-H., Vinegoni, C., Feruglio, P. F., Weissleder, R. and Tabin, C. J.** (2010). WNT5A/JNK and FGF/MAPK pathways regulate the cellular events shaping the vertebrate limb bud. *Curr. Biol.* **20**, 1993-2002.
**Gupta, V. and Poss, K. D.** (2012). Clonally dominant cardiomyocytes direct heart morphogenesis. *Nature* **484**, 479-484.
**Harrison, R. G.** (1918). Experiments on the development of the fore limb of Amblystoma, a self-differentiating equipotential system. *J. Exp. Zool.* **25**, 413-461.
**Heintzelman, K. F., Phillips, H. M. and Davis, G. S.** (1978). Liquid-tissue behavior and differential cohesiveness during chick limb budding. *J. Embryol. Exp. Morphol.* **47**, 1-15.
**Holt, M. and Oram, S.** (1960). Familial heart disease with skeletal malformations. *Heart* **22**, 236-242.
**Jovelin, R., He, X., Amores, A., Yan, Y.-l., Shi, R., Qin, B., Roe, B., Cresko, W. A. and Postlethwait, J. H.** (2007). Duplication and divergence of fgf8 functions in teleost development and evolution. *J. Exp. Zool. B Mol. Dev. Evol.* **308B**, 730-743.
**Keegan, B. R., Feldman, J. L., Begemann, G., Ingham, P. W. and Yelon, D.** (2005). Retinoic acid signaling restricts the cardiac progenitor pool. *Science* **307**, 247-249.
**Knezevic, V., De Santo, R., Schughart, K., Huffstadt, U., Chiang, C., Mahon, K. A. and Mackem, S.** (1997). Hoxd-12 differentially affects preaxial and postaxial chondrogenic branches in the limb and regulates Sonic hedgehog in a positive feedback loop. *Development* **124**, 4523-4536.
**Krawchuk, D., Weiner, S. J., Chen, Y.-T., Lu, B. C., Costantini, F., Behringer, R. R. and Laufer, E.** (2010). Twist1 activity thresholds define multiple functions in limb development. *Dev. Biol.* **347**, 133-146.
**Lewandoski, M., Sun, X. and Martin, G. R.** (2000). Fgf8 signalling from the AER is essential for normal limb development. *Nat. Genet.* **26**, 460-463.
**Li, Q. Y., Newbury-Ecob, R. A., Terrett, J. A., Wilson, D. I., Curtis, A. R. J., Yi, C. H., Gebuhr, T., Bullen, P. J., Robson, S. C., Strachan, T. et al.** (1997). Holt-Oram syndrome is caused by mutations in TBX5, a member of the Brachyury (T) gene family. *Nat. Genet.* **15**, 21-29.
**McDermott, D. A., Bressan, M. C., He, J., Lee, J. S., Aftimos, S., Brueckner, M., Gilbert, F., Graham, G. E., Hannibal, M. C., Innis, J. W. et al.** (2005). TBX5 genetic testing validates strict clinical criteria for Holt-Oram syndrome. *Pediatr. Res.* **58**, 981-986.
**McMahon, C., Gestri, G., Wilson, S. W. and Link, B. A.** (2009). Lmx1b is essential for survival of periocular mesenchymal cells and influences Fgf-mediated retinal patterning in zebrafish. *Dev. Biol.* **332**, 287-298.
**Mercader, N., Fischer, S. and Neumann, C. J.** (2006). Prdm1 acts downstream of a sequential RA, Wnt and Fgf signaling cascade during zebrafish forelimb induction. *Development* **133**, 2805-2815.
**Molven, A., Wright, C. V., Bremiller, R., De Robertis, E. M. and Kimmel, C. B.** (1990). Expression of a homeobox gene product in normal and mutant zebrafish embryos: evolution of the tetrapod body plan. *Development* **109**, 279-288.
**Moon, A. M. and Capecchi, M. R.** (2000). Fgf8 is required for outgrowth and patterning of the limbs. *Nat. Genet.* **26**, 455-459.
**Nasevicius, A. and Ekker, S. C.** (2000). Effective targeted gene 'knockdown' in zebrafish. *Nat. Genet.* **26**, 216-220.
**Neumann, C. J., Grandel, H., Gaffield, W., Schulte-Merker, S. and Nüsslein-Volhard, C.** (1999). Transient establishment of anteroposterior polarity in the zebrafish pectoral fin bud in the absence of sonic hedgehog activity. *Development* **126**, 4817-4826.
**Ng, J. K., Kawakami, Y., Büscher, D., Raya, A., Itoh, T., Koth, C. M., Rodríguez Esteban, C., Rodríguez-León, J., Garrity, D. M., Fishman, M. C. et al.** (2002). The limb identity gene Tbx5 promotes limb initiation by interacting with Wnt2b and Fgf10. *Development* **129**, 5161-5170.
**Ohuchi, H., Nakagawa, T., Yamamoto, A., Araga, A., Ohata, T., Ishimaru, Y., Yoshioka, H., Kuwana, T., Nohno, T., Yamasaki, M. et al.** (1997). The mesenchymal factor, FGF10, initiates and maintains the outgrowth of the chick limb bud through interaction with FGF8, an apical ectodermal factor. *Development* **124**, 2235-2244.
**Picker, A., Roellig, D., Pourquié, O., Oates, A. C. and Brand, M.** (2009). Tissue micromanipulation in zebrafish embryos. *Methods Mol. Biol.* **546**, 153-172.
**Rallis, C., Bruneau, B. G., Del Buono, J., Seidman, C. E., Seidman, J. G., Nissim, S., Tabin, C. J. and Logan, M. P. O.** (2003). Tbx5 is required for forelimb bud formation and continued outgrowth. *Development* **130**, 2741-2751.
**Searls, R. L. and Janners, M. Y.** (1971). The initiation of limb bud outgrowth in the embryonic chick. *Dev. Biol.* **24**, 198-213.
**Sun, X., Mariani, F. V. and Martin, G. R.** (2002). Functions of FGF signalling from the apical ectodermal ridge in limb development. *Nature* **418**, 501-508.
**Swett, F. H.** (1923). The prospective significance of the cells contained in the four quadrants of the primitive limb disc of Amblystoma. *J. Exp. Zool.* **37**, 207-217.
**Takeuchi, J. K., Koshiba-Takeuchi, K., Suzuki, T., Kamimura, M., Ogura, K. and Ogura, T.** (2003). Tbx5 and Tbx4 trigger limb initiation through activation of the Wnt/Fgf signaling cascade. *Development* **130**, 2729-2739.
**Vogel, A., Rodriguez, C. and Izpisúa-Belmonte, J. C.** (1996). Involvement of FGF-8 in initiation, outgrowth and patterning of the vertebrate limb. *Development* **122**, 1737-1750.
**Westerfield, M.** (2007). *The Zebrafish Book: A Guide for the Laboratory Use of Zebrafish (Danio rerio)*. Eugene, OR, USA: University of Oregon Press.
**Wyngaarden, L. A., Vogeli, K. M., Ciruna, B. G., Wells, M., Hadjantonakis, A.-K. and Hopyan, S.** (2010). Oriented cell motility and division underlie early limb bud morphogenesis. *Development* **137**, 2551-2558.
**Zhang, Z., Sui, P., Dong, A., Hassell, J., Cserjesi, P., Chen, Y.-T., Behringer, R. R. and Sun, X.** (2010). Preaxial polydactyly: interactions among ETV, TWIST1 and HAND2 control anterior-posterior patterning of the limb. *Development* **137**, 3417-3426.

# SUPPLEMENTAL FIGURES

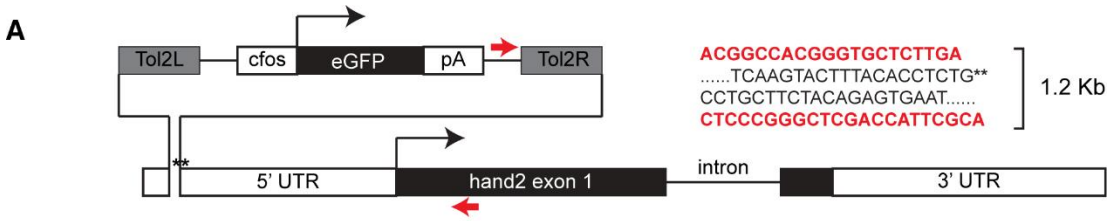


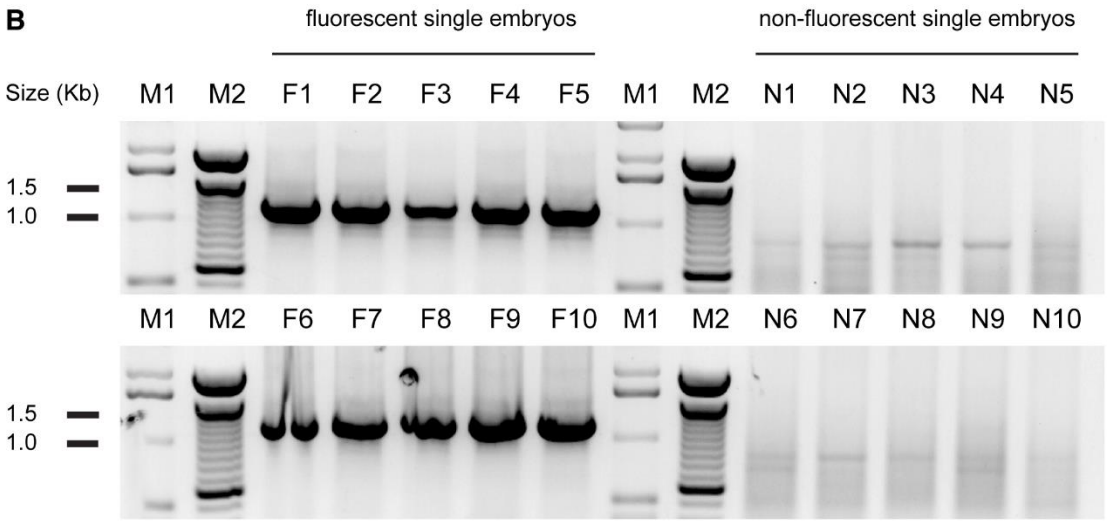


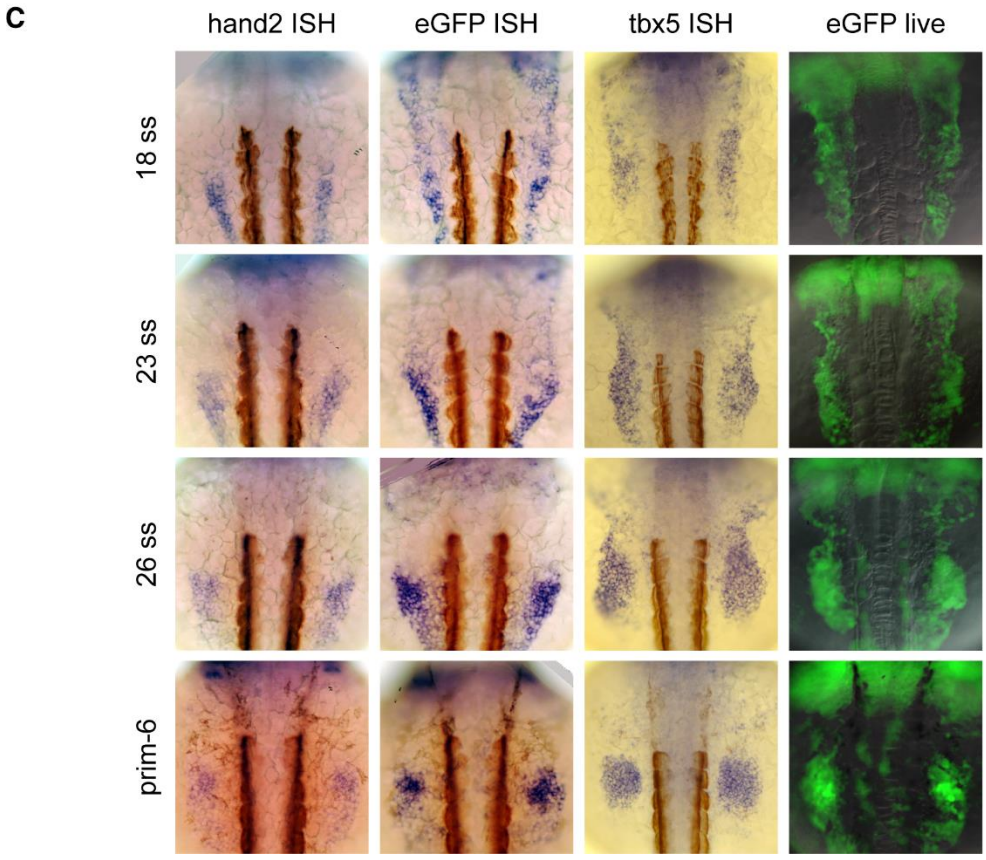

**Figure S1. Et(hand2:eGFP)ch2 is a hand2 enhancer-trap line**
A) Location and structure of the Tol2 transposon in *hand2* 5'-UTR. Paired red arrows show primers for the genotyping PCR and correspond to sequences highlighted in red.
B) Single-embryo genotyping PCR shows presence of 1.2 kb band in 10 embryos with hand2:eGFP fluorescence and a lack thereof in 10 non-fluorescent siblings.
C) Expression patterns of *hand2* mRNA, *egfp* mRNA, *tbx5* mRNA and eGFP protein in the pectoral limb field during limb bud initiation. Note the resemblance between *hand2* mRNA and *egfp* mRNA expression patterns, as well as that between *tbx5* mRNA and eGFP protein expression patterns. Dorsal view, anterior up.

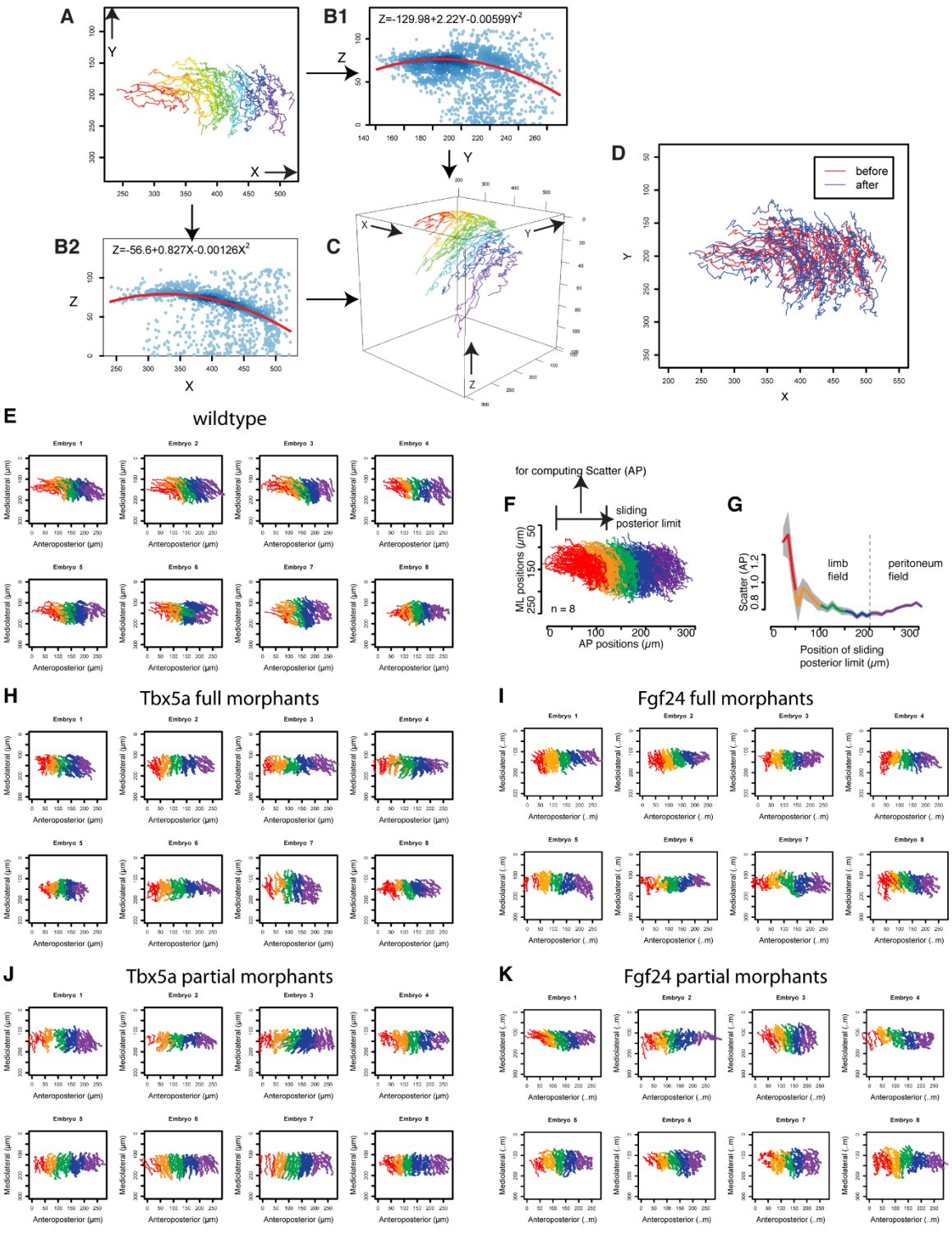

**Figure S2. (related to Figure 2, 3, 4). A semi-automatic 4D cell tracking procedure**
A) 2D cell tracks with (X, Y) coordinates are generated from the maximum intensity projection of confocal Z-stacks with the FIJI Manual Tracking plugin.
B1, B2) The Z coordinate for each (X, Y) is retrieved from the original Z-stacks by a custom automatic tracking ImageJ macro. A parabolic regression line is then fitted to entire sets of (X,Z) or (Y,Z) coordinates with a noise-resistant regression procedure (Rousseeuw and Leroy, 2005).
C) Reconstructed 3D tracks shown in (X, Y, Z).
D) Comparison between the original (X,Y) tracks (red) with the flattened (X, Y) tracks converted from the 3D tracks in C) (blue) following the Digital Flat Mount procedure.
E, H-K) shows cell tracks from individual embryos of 8 wildtype E), 8 Tbx5a full morphants H), 8 Fgf24 full morphants I), 8 Tbx5a partial morphants J), and 8 Fgf24 partial morphants K). Tracks are color-coded according to the somite level at which the track originated: red, orange, green, blue, and purple represent somite levels 1, 2, 3, 4, 5 and more posterior, respectively.
F) In the wildtype dataset, a group of cell tracks between a constant anterior limit and a sliding posterior limit are used to compute the Scatter value along the AP axis. Color code follows E).
G) The AP Scatter value plotted against the position of the sliding posterior limit used compute that AP Scatter value. Dashed line in B indicates the position of lowest AP Scatter value. Color code follows E).

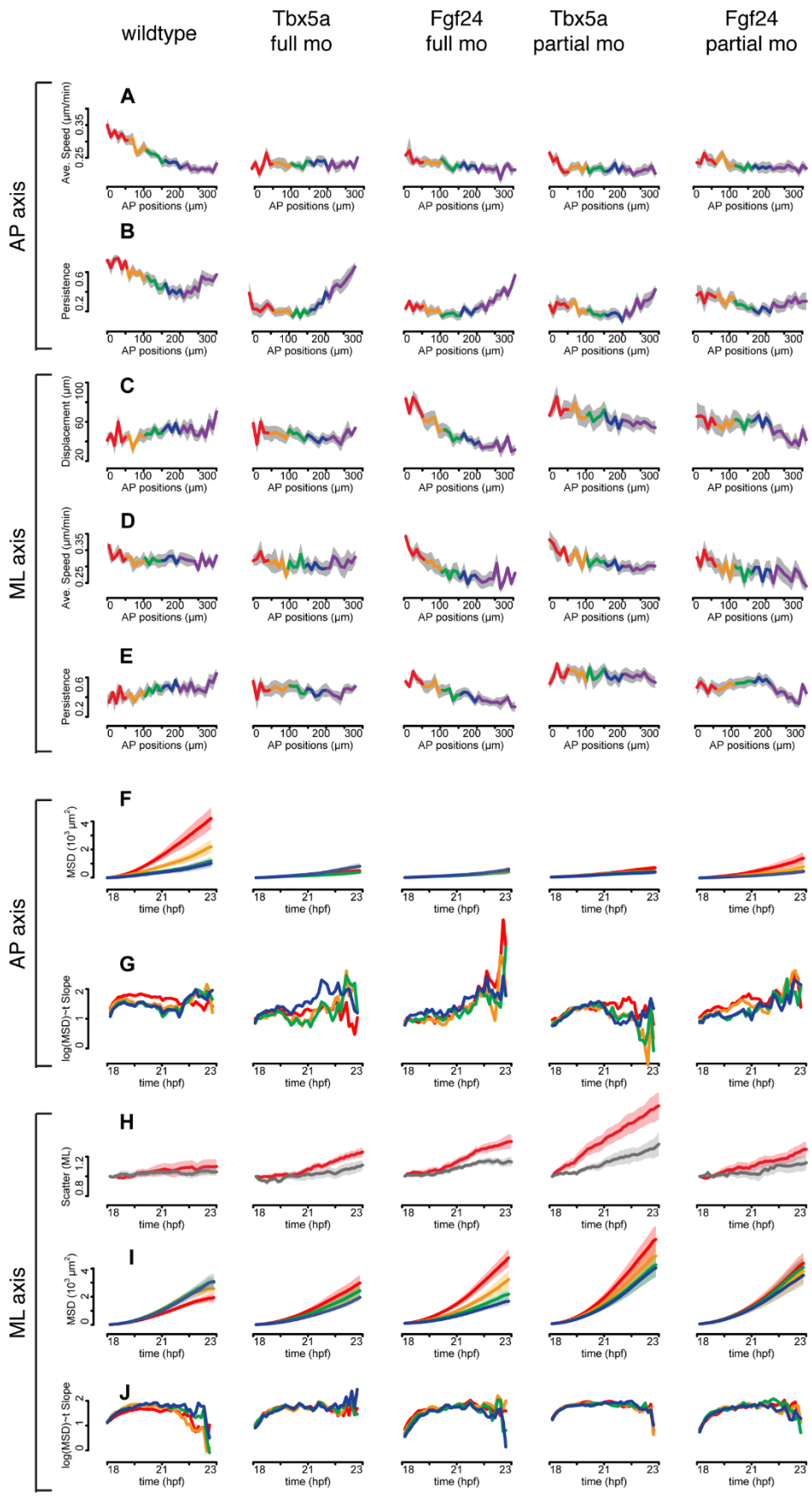

**Figure S3 (related to Figures 2, 3, and 4). Additional motility parameters of limb field cells along the AP and ML axes in wildtype, Tbx5a full morphants, Fgf24 full morphants, Tbx5a partial morphants and Fgf24 partial morphants**

Row A): Average AP speed plotted against the AP axis.
Row B): AP Persistence plotted against the AP axis.
Row C): Displacement along the mediolateral axis (ML) plotted against the AP axis.
Row D): Average ML speed plotted against the AP axis.
Row E): ML Persistence plotted against the AP axis.
Row F): AP Mean Squared Displacement (MSD_AP) plotted against time.
Row G): Slope of log(MSD_AP) plotted against time.
Row H): Scatter along the ML axis plotted against time.
Row I): MSD along the ML axis (MSD_ML) plotted against time.
Row J): Slope of log(MSD_ML)~t plotted against time.
Color code follows that in Figure S2E.

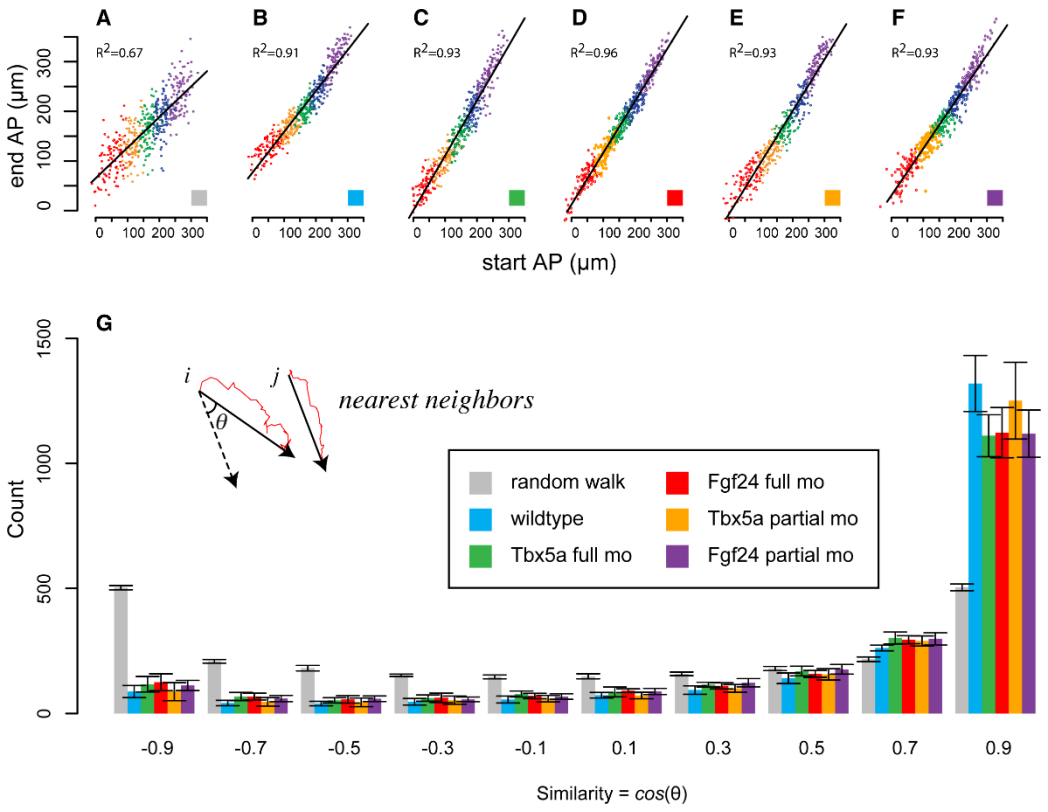


**Figure S4 (related to Figures 2 and 3). Spatiotopic migration of limb field cells is correlated with a constraint on motility angles between nearest neighbors**

A~F) Correlation between the start and the end AP positions of LPM cell tracks in wildtype B), Tbx5a full morphants C), Fgf24 full morphants D), Tbx5a partial morphants E), Fgf24 partial morphants F), and from a simulated 2D random walking group A). $R^2$ is the coefficient of determination.

G) Histogram of Similarity of nearest neighbors in wildtype, Tbx5a full morphants, Fgf24 full morphants, Tbx5a partial morphants, Fgf24 partial morphants, and from a simulated 2D random walk. Error bars indicate the 8-embryo standard error. i and j are in the schema are two nearest neighbors.

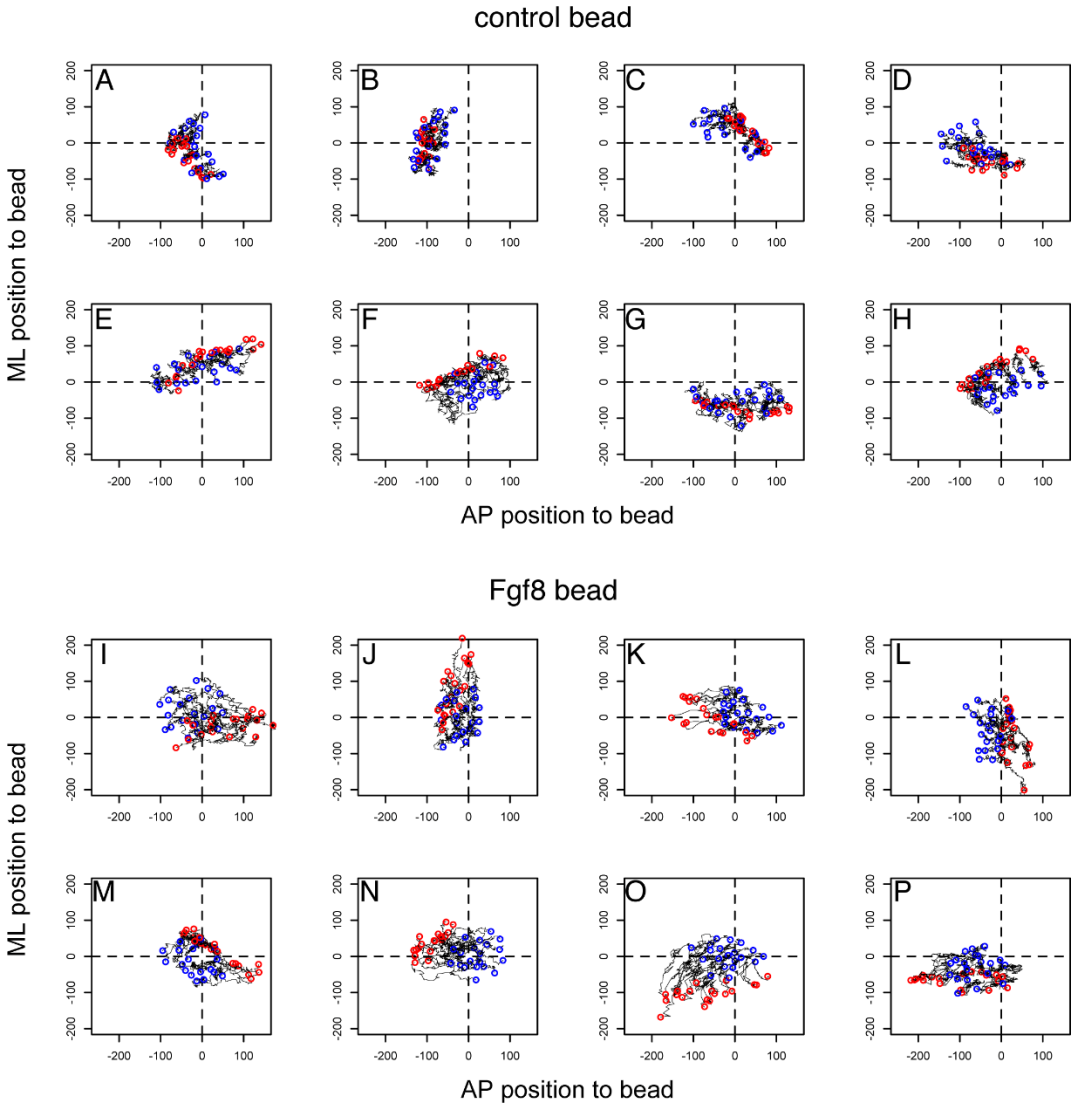


**Figure S5 (related to Figure 5). LPM cell tracks in bead-implanted Fgf24 morphant embryos.**
Circles highlight start (red) and end (blue) positions of each cell track in control bead (A-H) and Fgf8-coated bead (I-P) implanted embryos (n=20 cells per embryo). Units in each axis are in pixels (pixel size 0.8 µm in X and Y). Tracking time interval is 8 minutes/frame, with a total duration of 800 minutes.

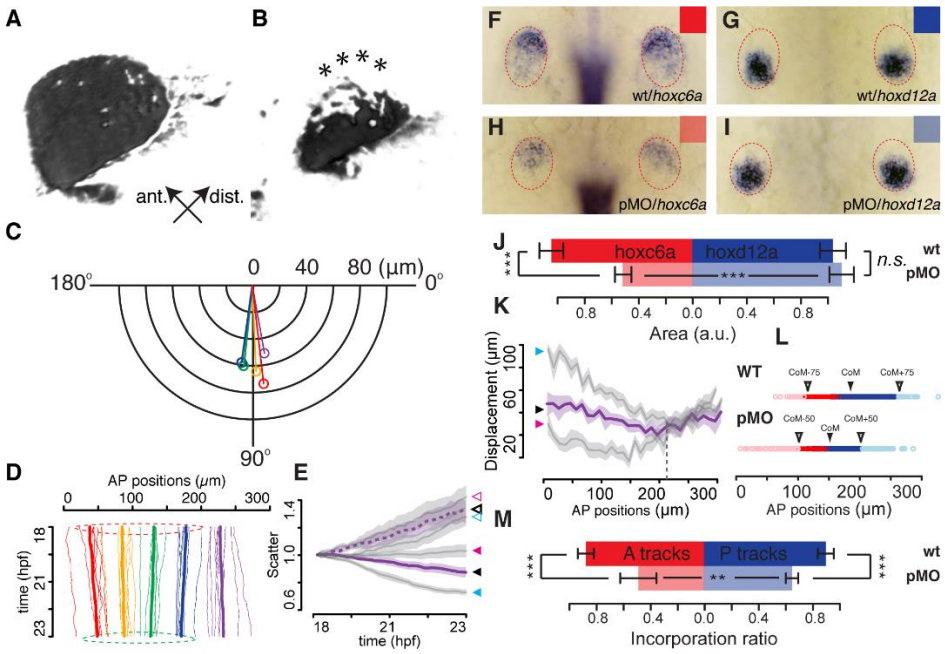


**Figure S6 (related to Figure 6). Incomplete cell convergence in the limb field of Fgf24 partial morphants correlates with observed anteriorly biased truncations in limb AP axis.**
A, B) Maximum intensity projections of the pectoral fin cartilaginous disc in a wildtype A) and an Fgf24 partial morphant B) 4 dpf larva. Arrows in A) show anterior and distal directions in A, B). Asterisks in B) highlight lesions on the anterior edge of the cartilaginous disc.
C) Polar plot showing the average orientation and magnitude of 2D displacement in 5 track groups subtracted by the average displacement of all LPM tracks in 8 Fgf24 partial morphant embryos.
D) Average net AP trajectories of 5 track groups subtracted by the average trajectories in all LPM tracks in 8 Fgf24 partial morphant embryos. Dotted circles highlight the similar sizes in limb field domains between tracks start (red) and end (green).
E) Scatter value along the AP axis plotted against time in 8 wildtype (blue arrowhead), 8 Fgf24 full Morphants (pink arrowhead), and 8 Fgf24 partial morphants (black arrowhead). Solid arrowhead: limb field. Open arrowhead: peritoneum field. Lines represent 8-embryo average; shaded areas represent 8-embryo standard error.
F-I) Expression patterns of *hoxc6a* (F, H) and *hoxd12a* (G, I) in 36 hpf limb buds of wildtype F, G) and Fgf24 partial morphant embryos H, I) (dorsal view, anterior up).
J) Quantification of expression areas of *hoxc6a* (red) and *hoxd12a* (blue) in wildtype (dark color) and Fgf24 partial morphants (light color) (n = 40 each). Wilcoxon test: p (hoxc6a wildtype-Fgf24 pMO) = $1.2 \times 10^{-13}$ (***), p (hoxd12a wildtype-Fgf24 pMO) = 0.3, p (hoxc6a Fgf24 pMO-hoxd12a Fgf24 pMO) = $2.2 \times 10^{-16}$ (***).
K) AP Displacement plotted against track start AP positions in 8 wildtype (blue arrowhead), 8 Fgf24 full morphants (green arrowhead), and 8 Fgf24 partial morphants (black arrowhead). Dotted vertical line represents the rough boundary at somite 4/5 between the limb field and the peritoneum field. Solid lines represent 8-embryo average; shaded areas represent 8-embryo standard error.

L) Track end AP positions of limb field tracks in 8 wildtype (wildtype) and 8 Fgf24 partial morphants (pMO). CoM: center of mass. CoM-75/CoM+75: anterior/posterior limits of the wildtype limb bud. CoM-34/CoM+34: anterior/posterior limits of the Fgf24 partial morphant limb bud.
M) Quantification of incorporation ratio of anterior (red, somites 1-2) and posterior (blue, somites 3-4) limb field tracks in wildtype (dark color) and Fgf24 partial morphants (light color) (n = 40 each). Wilcoxon test: p (A tracks wildtype-Fgf24 pMO) = $3.1 \times 10^{-4}$ (***), p(P tracks wildtype-Fgf24 pMO) = $1.6 \times 10^{-4}$ (***), p (A tracks Fgf24 pMO-P tracks Fgf24 pMO) = 0.02813 (*).

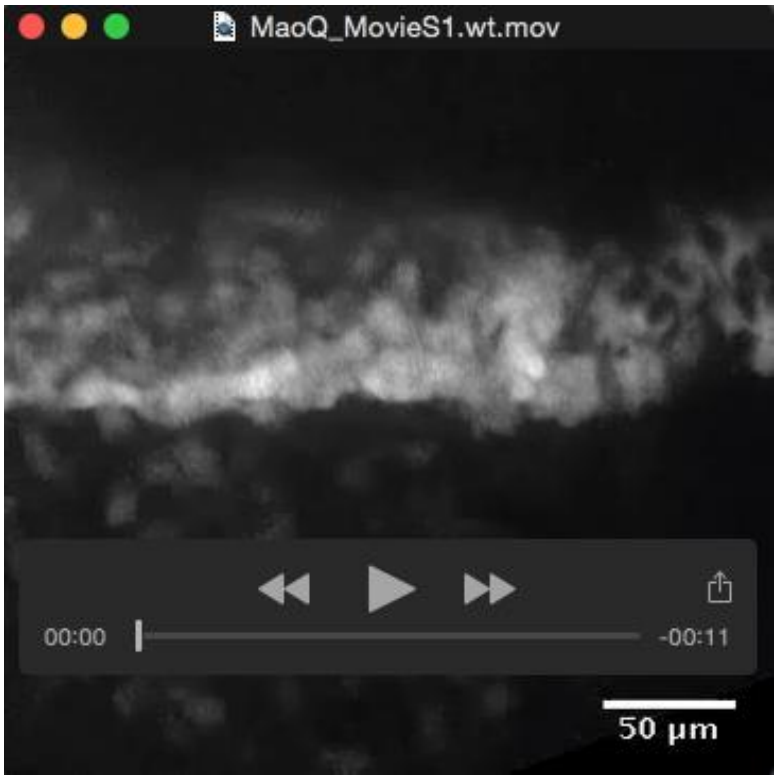


**Movie 1 (related to Figure 2). Asymmetric and spatiotopic convergence of limb field LPM cells in a wildtype embryo.** Time-lapse movie of a wildtype *Et(hand2:eGFP)ch2*; *Tg(h2afx:h2afv-mCherry)mw3* embryo, as shown in Figure 2A/A'~D/D'. Time interval: 8 min.

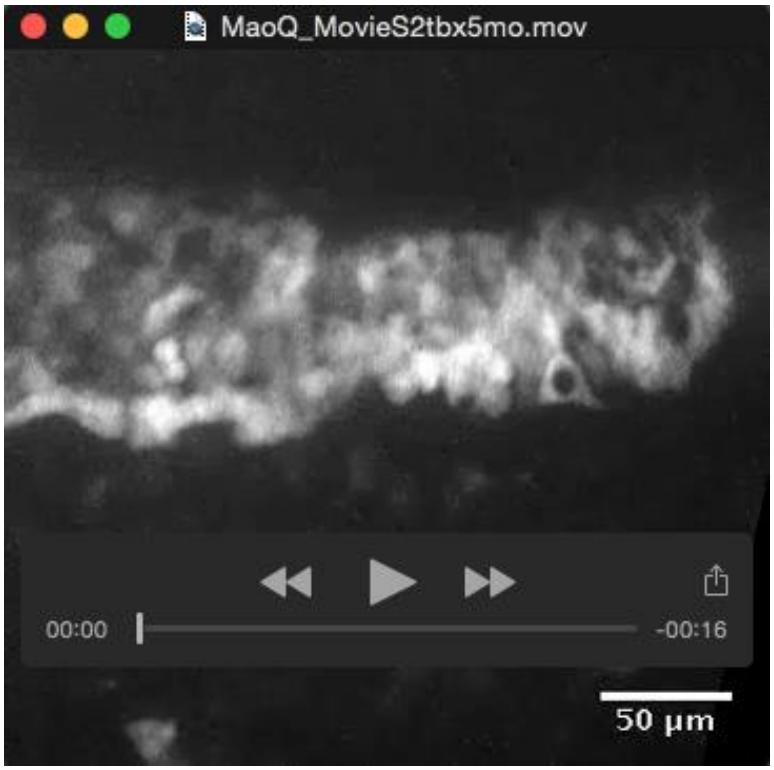


**Movie 2 (related to Figure 3). Lack of convergence, but maintenance of migration spatiotopicity, in limb field LPM cells in a Tbx5a full morphant embryo.** Time-lapse movie of a Tbx5a full morphant *Et(hand2:eGFP)ch2*; *Tg(h2afx:h2afv-mCherry)mw3* embryo, as shown in Figure 3A/A'~D/D'. Time interval: 8 min.

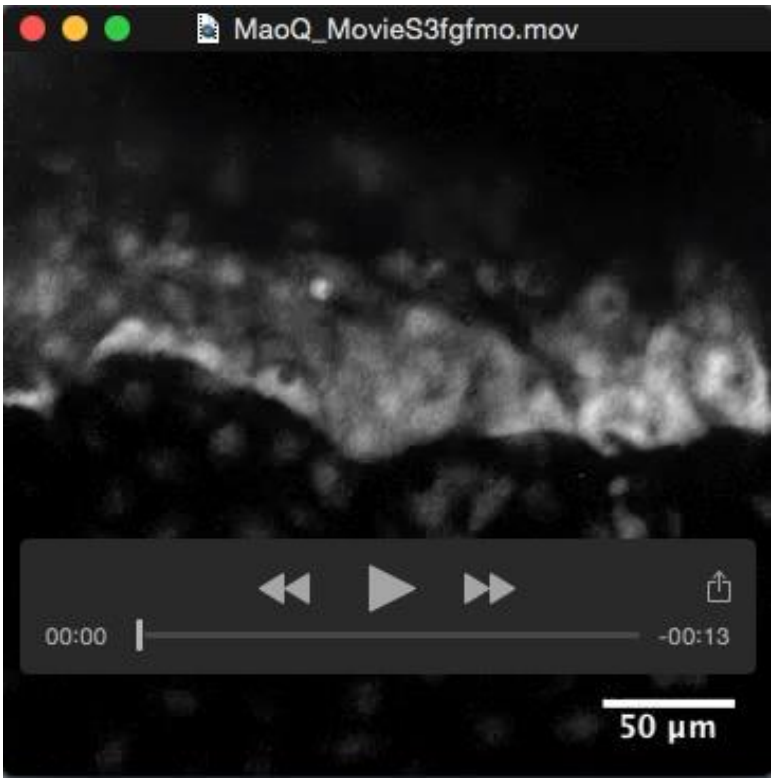


**Movie 3 (related to Figure 4). Lack of convergence, but maintenance of migration spatiotopicity, in limb field LPM cells in an Fgf24 full morphant embryo.** Time-lapse movie of a Fgf24 full morphant *Et(hand2:eGFP)ch2*; *Tg(h2afx:h2afv-mCherry)mw3* embryo, as shown in Figure 4A/A'~D/D'. Time interval: 8 min.

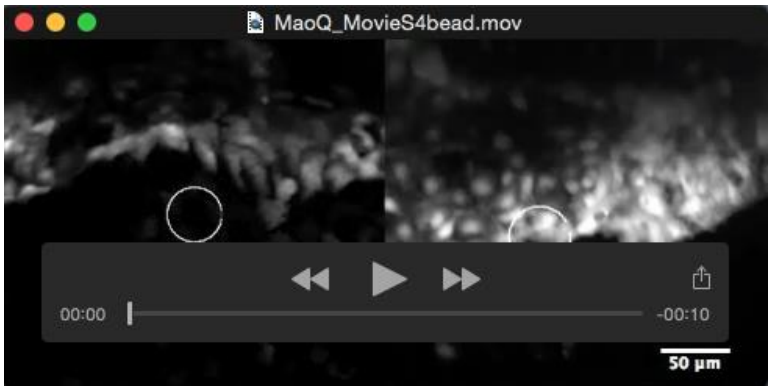


**Movie 4 (related to Figure 5). Convergence of limb field LPM cells towards an Fgf source.** Time-lapse movie of a Fgf24 full morphant *Et(hand2:eGFP)ch2*; *Tg(h2afx:h2afv-mCherry)mw3* embryo with a BSA (A) or Fgf8b (B)-coated bead (heighted in a white circle). Time interval: 8 min.

## SUPPLEMENTAL EXPERIMENTAL PROCEDURES

### Generation of Et(hand2:eGFP)ch2

*Et(hand2:eGFP)ch2* (D.G. Ahn, University of Chicago, present address: Department of Biology, Chungnam National University, Daejeon, Republic of Korea) was recovered from a Tol2 enhancer trap screen based on eGFP expression pattern and outcrossed to *AB wildtype individuals for more than three generations to ensure the observed eGFP expression pattern was associated with a single-insertion site. The Tol2 transposon plasmid used for this screen, pT2KXIGΔ, is as described in (Urasaki et al., 2006). The transposon insertion site in *Et(hand2:eGFP)ch2* is mapped at the 5' UTR of *hand2* with the PCR-based Universal Fast Walking method, as described in (Myrick and Gelbart, 2002), then further confirmed with regular PCR (Figure S1). *Et(hand2:eGFP)ch2* is maintained and used as hemizygotes to control for any potential deleterious effects of the transgenic insertion.

## Morpholinos

The antisense oligonucleotide (morpholino) used in this study against *tbx5a* (5'-CCTGTACGATGTCTACCGTGAGGC-3') is as described in (Ahn et al., 2002). The dose of morpholino per injection is measured following the protocol recommended by Gene Tools, LLC. The morpholino concentration is titrated such that we achieve 100% pectoral fin absence using the lowest possible dose, which was determined to be 1 ng per embryo for our anti-*tbx5a* morpholino.

## mRNA *in situ* hybridization and immunochemistry

DIG-labeled antisense riboprobe were generated based on *tbx5a*, *hand2*, and *egfp* mRNA sequences (Roche Applied Science). Chromogenic antibody staining was performed as described in (Skromne et al., 2007) with the following modifications: primary mouse anti-myosin heavy chain antibody (A4.1025, Developmental Studies, Hybridoma Bank, IA, USA) was used at a dilution of 1:100; secondary peroxidase-labeled anti-mouse IgG (H+L) antibody (Vector laboratories, PI-2000) was use at a dilution of 1:200. DAB color product was developed with the Peroxidase Substrate Kit (Vector laboratories, SK-4100).

## Trajectory analyses

The final tracking dataset contains the following parameters: AP position (x), ML position (y), time (t) and track serial (tr). From these four variables, we further calculated the following variables: Scatter, Displacement, Instantaneous Speed, Average Speed, Persistence, MSD, and Similarity between nearest neighbors. The mathematical definition for each variable is listed as follows. All calculation and data visualization were performed using R software (Team).

***Scatter.*** Scatter is defined as the standard deviation of x (or y) of a given group of points at a given time point (t = i), divided by the standard deviation of x (or y) of the same group of points at the starting point (t = 1) (formula 1a for x, formula 1b for y). Therefore, Scatter is a measure of the fold change of "scattering" of a group of spots compared to their starting positions. Scatter is expressed either as a function of time, or as a function of AP positions:

$$Scatter.x(x=i,t=j)=\frac{\sigma(x_{x=1:i,t=j})}{\sigma(x_{x=1:i,t=1})} \quad (1a)$$

$$Scatter.y(x=i,t=j)=\frac{\sigma(y_{x=1:i,t=j})}{\sigma(y_{x=1:i,t=1})} \quad (1b)$$

The Scatter value along the AP axis (Scatter x) is used to partition the limb field and the peritoneum field. As shown in Figure S4, as the posterior limit of track groups used for calculating Scatter x expands posteriorly, Scatter x value at 23 hpf drops to the lowest at around 200 μm along the AP axis (roughly correlated with the boundary between somite 4~5), suggesting that cells posterior to this position (peritoneum) fail to converge with more anterior cells (limb field).

***Displacement.*** Displacement is defined as the overall change of x (or y) of a given track spot between the start (t = 1) and the end of the track (t = 40) (formula 2a for x, formula 2b for y). Displacement is expressed as a function of track origin:

$$Displacement\_x(x,t=1) = x_{x,t=40} - x_{x,t=1} \qquad (2a)$$

$$Displacement\_y(x,t=1) = y_{x,t=40} - y_{x,t=1} \qquad (2b)$$

***Speed. Instantaneous Speed*** is defined as the change of *x* (or *y*) of a given track spot between two consecutive time points (formula 3a for *x*, formula 3b for *y*). ***Average Speed*** is the mean of Instantaneous Speed for a given track spot across all time points.

$$Inst\_speed\_x(x,t=i) = x_{x,t=i+1} - x_{x,t=i} \qquad (3a)$$

$$Inst\_speed\_y(x,t=i) = y_{x,t=i+1} - y_{x,t=i} \qquad (3b)$$

$$Ave\_speed\_x(x) = \frac{1}{39}\sum_{i=1}^{40}(x_{x,t=i+1} - x_{x,t=i}) \qquad (4a)$$

$$Ave\_speed\_y(x) = \frac{1}{39}\sum_{i=1}^{40}(y_{x,t=i+1} - y_{x,t=i}) \qquad (4b)$$

***Persistence.*** Persistence is defined as the ratio of Displacement over the overall trajectory length for a given track along the AP or ML axis (formula 5a for *x*, formula 5b for *y*). Persistence roughly describes the efficiency of cell migration along a given direction (Persistence = 1 means the cell migrates in a straight line, Persistence = 0 means the cell returns to its original position). However, Persistence is limited by that it does not consider the intermediate migration process, and thus cannot distinguish between, for example, random walk or back-and-forth directional movement. This limitation can be resolved by calculating MSD.

$$Persistence\_x(x) = \frac{x_{x,t=40} - x_{x,t=1}}{\sum_{i=1}^{40}(x_{x,t=i+1} - x_{x,t=i})} \qquad (5a)$$

$$Persistence\_y(x) = \frac{y_{x,t=40} - y_{x,t=1}}{\sum_{i=1}^{40}(y_{x,t=i+1} - y_{x,t=i})} \qquad (5b)$$

***MSD (Mean Square Displacement)***. The formula for MSD is described in 6a (for *x*) and 6b (for *y*). N represents total number of time points. n represents current number of time points since the starting point. Δt represents the interval between two consecutive time points. The shape of the MSD~n function (equals MSD~t) describes the mode of migration, as MSD increases linearly with time during random walk, and quadraticly with time in directional migration (Berg, 1993; Codling et al., 2008). Thus on the logarithmic scale, MSD~time function has a slope of 1 during random walk, and 2 during directional migration.

$$MSD.x(n) = \frac{1}{N-n}\sum_{i=1}^{N-n}[x_{(n+i)\Delta t} - x_{i\Delta t}]^2 \qquad (6a)$$

$$MSD.y(n) = \frac{1}{N-n}\sum_{i=1}^{N-n}[y_{(n+i)\Delta t} - y_{i\Delta t}]^2 \qquad (6b)$$

MSD increases linearly with time during a random walk, but quadratically with time during directional migration bouts (Berg, 1993; Codling et al., 2008). Figure S3F shows that tracking groups 1 (red) and, to a lesser extent, tracking group 2 (yellow) exhibit significantly higher MSD values over time compared to other tracking groups, indicating a higher degree of directional migration exhibited by these anterior LPM cells. We further quantified the slope value in linear model log(MSD)~time. A slope for log(MSD)~time equaling 1 suggests random walk, whereas a slope equaling 2 is indicative of directional migration. We observed an the elevated slope value in linear model log(MSD)~time between track group 1 and the rest of limb field cells (Figure S3G), suggesting a more directional motion pattern in track group 1 cells. Strikingly, in full or partial morphants for Tbx5a or Fgf24, this anterior elevation of AP cell motility, as measured by Displacement, Average Speed, Persistence and MSD, is lost or diminished (Figure 3J, Figure 4K, Figure S3A1-D1, A2-D2). This suggests that Tbx5a and Fgf24 are required for the directional convergent motility of the anterior-most LPM cells along the AP axis. Same sets of measurements along the orthogonal axis (mediolateral axis, ML) are also presented (Figure S3C-E, H-J). Interestingly, we observed a descending trend of ML motility along the AP axis in Fgf24 full morphants (Figure S3C-E, third column), reminiscent of the descending trend of ML motility along the AP axis in wildtype embryos. This might reflect a redirection of cell motility in the anterior-most LPM cells from caudal-oriented to lateral-oriented upon loss of the convergent cue Fgf24.

***Similarity.*** The motion similarity between nearest neighbors i and j is defined as the cosine value of the angle formed between their instantaneous velocities. Similarity can be expressed as a function of time or nearest neighbor pairs. In the case of independent random walk, the histogram of similarity is symmetrical on either side of 0 degree, representing equal probability of two nearest neighbors going parallel or anti-parallel.

$$Similarity_{ij}(t) = \cos(\arctan(\frac{y_{i,t+1} - y_{i,t}}{x_{i,t+1} - x_{i,t}}) - \arctan(\frac{y_{j,t+1} - y_{j,t}}{x_{j,t+1} - x_{j,t}})) \quad (7)$$

***Center of Mass and defining the limb bud region.*** The wildtype limb bud region is defined as the region within ±75 μm to the average end positions of all limb field tracks (**Center of Mass**). The expression area of *hoxc6a* and *hoxd12a* in wildtype and Tbx5a partial morphants indicates that the size of limb bud in Tbx5a partial morphants is roughly 45% of the wildtype limb bud size. The Tbx5a partial morphant limb bud region is thus defined as the region within ±34 μm to the average end positions of all limb field tracks.

***Incorporation ratio.*** The Incorporation ratio is defined as the ratio of tracks from a given AP region that end up in the limb bud region over all tracks from the same AP region. For

instance, the Incorporation ratio of anterior limb field tracks are defined as all tracks that are from the anterior limb field (from somite levels 1 and 2) that ends up in the limb bud region divided by all tracks from the anterior limb field. The Incorporation ratio of posterior limb field tracks are defined as all tracks that are from the posterior limb field (from somite levels 3 and 4) that ends up in the limb bud region divided by all tracks from the posterior limb field.

**Simulation of a 2D random walk population**

The highly spatiotopic LPM cell migration lead us to speculate that this might be a form of collective cell migration (Friedl and Gilmour, 2009; Rørth, 2009). To investigate whether individual LPM cells are constrained in their motility, we compared the observed LPM cell motility with that from a simulated 2D random walking population (Figure S4). We first compared the correlation between the start and the end positions between the observed conditions (Figure S4B-F) and the simulated condition (Figure S4A). While the coefficient of determination ($R^2$) is comparable between all experimental conditions (Figure S4B-F), it is much lower in the simulated 2D random walk population (Figure S4A), indicating LPM cell migration has higher spatiotopicity than would be seen if cells were undergoing a random walk. We then tested if the angles between the instantaneous velocities of nearest neighbors are comparable in all conditions. In the Similarity histogram, we observed a strong bias towards smaller angles (Similarity close to 1) in wildtype, Tbx5a full morphants and Tbx5a partial morphants, in contrast to the symmetrical distribution in the 2D random walk population (Figure S4E, Kolmogorov-Smirnov Test: Simulated~WT: $p < 2.2 \times 10^{-16}$). This indicates certain similarity and thus coordination in motility directions between nearest neighbors in all experimental conditions.

The 2D random walk population was simulated in the following steps:

1) Assign the start positions of the population the identical start positions of the wildtype population;
2) For each instantaneous migration step, assign instantaneous speeds randomly chosen from distributions with parameters comparable to the observed corresponding values in the wildtype dataset, and angles randomly chosen from a uniform distribution of [0, pi] (assuming LPM cells do not cross the midline).

## SUPPLEMENTAL REFERENCES

Ahn, D.-G., Kourakis, M.J., Rohde, L.A., Silver, L.M., and Ho, R.K. (2002). T-box gene tbx5 is essential for formation of the pectoral limb bud. Nature *417*, 754–758.

Berg, H. (1993). Random Walks in Biology (Princeton University Press).

Codling, E.A., Plank, M.J., and Benhamou, S. (2008). Random walk models in biology. J R Soc Interface *5*, 813–834.

Friedl, P., and Gilmour, D. (2009). Collective cell migration in morphogenesis, regeneration and cancer. Nat Rev Mol Cell Biol *10*, 445–457.

Myrick, K.V., and Gelbart, W.M. (2002). Universal Fast Walking for direct and versatile determination of flanking sequence. Gene *284*, 125–131.

Rousseeuw, P.J., and Leroy, A.M. (2005). Robust Regression and Outlier Detection (Wiley).

Rørth, P. (2009). Collective cell migration. Annu Rev Cell Dev Biol *25*, 407–429.

Skromne, I., Thorsen, D., Hale, M., Prince, V.E., and Ho, R.K. (2007). Repression of the hindbrain developmental program by Cdx factors is required for the specification of the vertebrate spinal cord. Development *134*, 2147–2158.

Team, R.C. R: A language and environment for statistical computing. www.R-Project.org.

Urasaki, A., Morvan, G., and Kawakami, K. (2006). Functional Dissection of the Tol2 Transposable Element Identified the Minimal cis-Sequence and a Highly Repetitive Sequence in the Subterminal Region Essential for Transposition. Genetics *174*, 639–649.